Rigid NON- and NSN-Ligand Complexes of Tetravalent and Trivalent Uranium: Comparison of U–OAr_2 and U–SAr_2 Bonding

Balamurugan Vidjayacoumar,[a] *Sougandi Ilango,*[a] *Matthew J. Ray,*[a] *Terry Chu,*[a] *Kristopher B. Kolpin,*[a] *Nicholas R. Andreychuk,*[a] *Carlos A. Cruz,*[a] *David J. H. Emslie,**[,a] *Hilary A. Jenkins*[b] *and James F. Britten*[b]

[a] Department of Chemistry, McMaster University, 1280 Main Street West, Hamilton, ON, L8S 4M1, Canada. Fax: (905)-522-2509; Tel: (905)-525-9140 x 23307; E-mail: emslied@mcmaster.ca.

[b] McMaster Analytical X-Ray Diffraction Facility, Department of Chemistry, McMaster University, 1280 Main Street West, Hamilton, ON, L8S 4M1, Canada.

RECEIVED DATE

Abstract: A rigid NSN-donor proligand, 4,5-bis(2,6-diisopropylanilino)-2,7-di-*tert*-butyl-9,9-dimethylthioxanthene ($H_2[TXA_2]$, **1**) was prepared by palladium-catalyzed coupling of 2,6-diisopropylaniline with 4,5-dibromo-2,7-di-*tert*-butyl-9,9-dimethylthioxanthene. Deprotonation of **1** using ^{n}BuLi provided $Li_2(DME)_2[TXA_2]$ (**2**), and subsequent reaction with UCl_4 afforded $[Li(DME)_3][(TXA_2)UCl_3]$ (**4**). The analogous NON-donor ligated complex $[(XA_2)UCl_3K(DME)_3]$ [**3**; XA_2 = 4,5-bis(2,6-diisopropylanilino)-2,7-di-*tert*-butyl-9,9-dimethylxanthene] was prepared by reaction of $K_2(DME)_x[XA_2]$ with UCl_4. A cyclic voltammogram (CV) of **3** in THF/$[NBu_4][B(C_6F_5)_4]$ at 200 mVs^{-1} showed an irreversible reduction to uranium(III) at E_{pc} = –2.46 V versus $FeCp_2^{0/+1}$, followed by a product wave at $E_{1/2}$ = –1.83 V. Complex **4** also underwent irreversible reduction to uranium(III) [E_{pc} = –2.56 V], resulting in an irreversible product peak at E_{pa} = –1.83 V. One-electron reduction of complexes **3** and **4** using K(naphthalenide) under an argon atmosphere in DME yielded 6-coordinate $[(XA_2)UCl(DME)]$ (**5**) and thermally unstable 7-coordinate $[(TXA_2)U(DME)Cl_2Li(DME)_2]$ (**6**), respectively. The U–S distances in **4** and **6** are uncommonly short, the C–S–U angles are unusually acute, and the thioxanthene backbone of the TXA_2 ligand is significantly bent. By contrast, the xanthene backbone in XA_2 complexes **3** and **5** is planar. However, κ^3-coordination and an approximately meridional arrangement of the ancillary ligand donor atoms is maintained in all complexes. DFT and Atoms In Molecules (AIM) calculations were carried out on **3**, **4**, **5**, **6**, $[(XA_2)UCl_3]^-$ (**3B**), $[(TXA_2)UCl_2(DME)]^-$ (**6B**) and $[(TXA_2)UCl(DME)]$ (**6C**) to probe the extent of covalency in U–SAr_2 bonding relative to U–OAr_2 bonding.

Introduction

In *f*-element chemistry, the substitution of oxygen and nitrogen donors for heavier chalcogen or pnictogen elements is of importance for the development of new strategies for lanthanide/actinide separation in nuclear fuel reprocessing.[1-2] Given the successful application of the rigid, dianionic NON-donor ligand XA_2 [4,5-bis(2,6-diisopropylanilino)-2,7-di-*tert*-butyl-9,9-dimethylxanthene] for the synthesis of both thermally robust and highly reactive thorium(IV) complexes,[3-6] we became interested in the synthesis of uranium complexes of both the XA_2 ligand and the previously unreported NSN-donor analogue, TXA_2 (Figure 1).

The TXA_2 ligand is an example of a mixed hard/soft donor ligand. In transition metal and lanthanide chemistry, hard/soft amido/phosphine ligands have been exploited to great success by Fryzuk[7] and others,[8] and recently Kiplinger *et al.* reported a range of mono- and bis-ligand uranium halide complexes of the bis[2-(diisopropylphosphino)-4-methylphenyl]amido anion (PNP^1 in Figure 1). Most of these complexes exhibit κ^3*(PNP)*-coordination. However, κ^2*(PN)*-coordination was observed for both ligands in $[(PNP^1)_2UCl_2]$, and dissociation of at least one phosphine arm was proposed for $[(PNP^1)_2UI]$ in solution.[9] Edwards *et al.* also reported κ^2*(PN)*-coordination in $[\{(\kappa^2\text{-}L)_2An^{IV}Cl(\mu\text{-}Cl)\}_2]$ (An = Th, U) complexes of bis[2-(dialkylphosphino)ethyl]amido anions (PNP^2 in Figure 1), and a mixture of κ^2*(PN)*- and κ^1*(N)*-coordination was observed in $[(\kappa^2\text{-}L)(\kappa^1\text{-}L)_2An^{V}Cl_2]$ (An = Th, U; L = PNP^2).[10] By contrast, the rigidity of the TXA_2 thioxanthene backbone, combined with bulky *N*-aryl substituents, can be expected to ensure positioning of the soft neutral donor in the metal coordination sphere and disfavour the formation of bis- or tris-ligand complexes. The XA_2 and TXA_2 ligands therefore provide an opportunity to explore the extent to which the structures and redox behavior of uranium complexes are affected by donor atom substitution within a highly rigid framework.

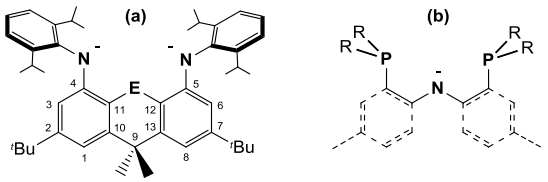

Figure 1. Structures of: (a) the XA_2 (E = O) and TXA_2 (E = S) dianions, and (b) the PNP[1] (Solid & dashed lines; R = ^{i}Pr) and PNP[2] (Solid lines; R = ^{i}Pr or Et) monoanions.

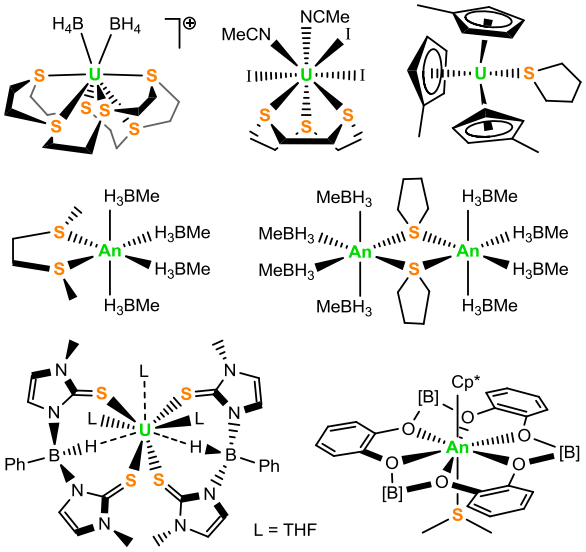

Figure 2. Structurally characterized non-uranyl actinide complexes containing soft neutral chalcogen donors (An = Th, U; [B] = BCat; Cat = *ortho*-$O_2C_6H_4$).

Only a small number of actinide complexes containing soft neutral chalcogen donors[11] have been reported. Crystallographically characterized non-uranyl examples include $[Cp^*An^{IV}\{\kappa^6\text{-}B_3(Cat)_6\}(SMe_2)]$ (An = Th, U; Cat = *ortho*-$O_2C_6H_4$],[12] $[(\kappa^2\text{-}MeSCH_2CH_2SMe)U^{IV}(BH_3Me)_4]$,[13] $[\{(MeBH_3)_4U^{IV}(\mu\text{-THT})\}_2]$

(THT = tetrahydrothiophene),[14] $[(C_5R_5)_3U^{III}(THT)]$,[15] $[(\kappa^3\text{-}9S3)An^{III}I_3(NCMe)_2]$ (An = U or Pu; 9S3 = 1,4,7-trithiacyclononane = 9-thiacrown-3),[16,17] and $[(\kappa^6\text{-}18S6)U^{III}(BH_4)_2][BPh_4]$ (18S6 = 18-thiacrown-6),[18] and $[\{\kappa^3\text{-}HRB(mim)_2\}_2U^{III}(THF)_3][BPh_4]$ (R = H or Ph; mim = *N*-methylthioimazolyl);[19] Figure 2.

Results and Discussion

Ligand Synthesis

The NSN-donor proligand 4,5-bis(2,6-diisopropylanilino)-2,7-di-*tert*-butyl-9,9-dimethyl-thioxanthene ($H_2[TXA_2]$; **1**; Figure 1) was synthesized by Hartwig-Buchwald coupling of 4,5-dibromo-2,7-di-*tert*-butyl-9,9-dimethyl-thioxanthene (prepared from thioxanthone)[20] with 2,6-diisopropylaniline (Scheme 1). Stirring $H_2[TXA_2]$ with 2.0 equivalents of *n*BuLi in DME at room temperature for 12 hours followed by evaporation to dryness then provided $Li_2(DME)_2[TXA_2]$ (**2**) as a yellow oil which resisted crystallization and was most conveniently generated and used *in situ*.

Scheme 1. Synthesis of $H_2[TXA_2]$ (**1**) and $Li_2(DME)_2[TXA_2]$ (**2**) [Ar = 2,6-diisopropylphenyl; DPEPhos = bis{2-(diphenylphosphino)phenyl}ether].

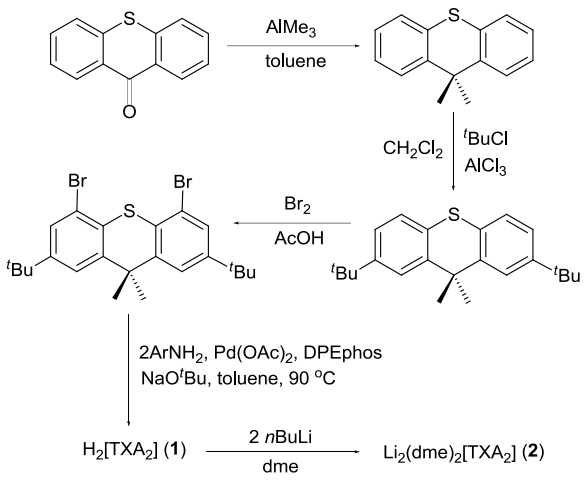

Uranium(IV) XA_2 and TXA_2 Complexes

Reaction of $K_2(DME)_x[XA_2]$ with UCl_4 in DME afforded the tetravalent uranium complex $[(XA_2)UCl_2(\mu\text{-}Cl)K(DME)_3]$ (**3**) as red-orange crystals in 75 % yield. Similarly, addition of a solution of $Li_2(DME)_2[TXA_2]$ (**2**) to UCl_4 in DME at –78 °C and stirring at room temperature for 12 hours provided highly soluble $[Li(DME)_3][(TXA_2)UCl_3]$ (**4**), which was isolated as a dark red solid in 42 % yield (Scheme 2). Complexes **3** and **4** were characterized by elemental analysis, ^{1}H NMR spectroscopy, UV-Visible-NIR spectroscopy, X-ray crystallography, and cyclic voltammetry.

Scheme 2. Synthesis of uranium(IV) complexes **3** and **4**. Tertiary-butyl groups are omitted for clarity.

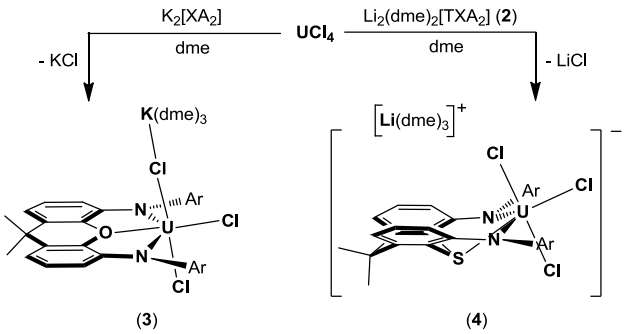

In the solid state (Figure 3; Table 1), complex **3** is a six coordinate 'ate' complex with a $K(DME)_3^+$ counterion coordinated to Cl(3); the K–Cl distance is 3.151(2) Å. X-ray crystal structures containing M–(μ-Cl)–$K(DME)_3$ linkages have not previously been reported, although comparable K–Cl distances are observed in [{κ^2-$CH_2(C_6R_4O\text{-}2)_2$}$_2$Th(κ^1-DME)(μ-Cl)K$(DME)_2$] [3.127(2) Å],[21] [Cp_3Ho(μ-Cl)K(18-C-6)] [3.131 and 3.151 Å],[22] and [{κ^3-$C_6R_3O(CH_2C_6R_4O\text{-}2)\text{-}2,6$}Ta(μ-Cl)$_2K(DME)_2$}$_2$($OCH_2CH_2O$)] [3.166(3) and 3.196(3) Å].[23] As a result of $K(DME)_3^+$ coordination in **3**, U–Cl(3) is elongated to 2.672(1) Å, relative to U–Cl(2) and U–Cl(3) [2.597(1) and 2.619(1) Å, respectively]. Longer U–Cl distances of 2.707(5) Å, 2.700(5) Å (bridging) and 2.648(5) Å (terminal) were observed in related [{κ^3-$O(CH_2CH_2NAr)_2$}UCl(μ-Cl)$_2$Li$(THF)_2$] (Ar = 2,6-diisopropylphenyl),[24] perhaps due to closer approach of the amido donors in the latter more flexible NON-donor ligand; U–N_{avg} is 2.19 Å, versus 2.30 Å in **3**. However, a wide range of U^{IV}–NR_2 bond distances have been reported, for example 2.18(2)–2.19(2) Å in [{κ^3-$O(SiMe_2N^tBu)_2$}UI(μ-I)$_2$Li$(THF)_2$],[24] 2.21(2)–2.35(2) Å in [$U(NPh_2)_4$],[25] 2.23(1) Å in [(κ^3-Tp')$UCl_2(NPh_2)$],[26] 2.29(1) Å in [$Cp_3U(NPh_2)$],[27] and 2.343(7) and 2.411(3) Å in [(PNP^1)UCl_3(L)] (L = THF or $OPPh_3$).[9]

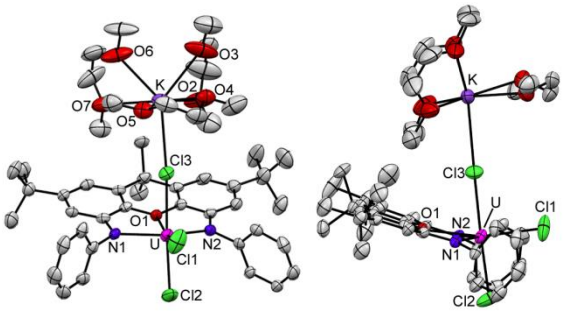

Figure 3. Molecular structure of **3** with thermal ellipsoids at 50% probability. Hydrogen atoms, isopropyl groups, and lattice solvent are omitted for clarity.

The U–O distance in **3** is 2.465(3) Å, which is very similar to the U–$O_{dialkylether}$ bond of 2.43(1) Å in [{κ^3-O($CH_2CH_2NAr)_2$}UCl(μ-Cl)$_2$Li$(THF)_2$] (Ar = 2,6-diisopropylphenyl).[24] Electronically more comparable uranium diarylether complexes have not been structurally characterized, but U–OArMe distances in simple halide or acetylacetonate uranium(IV) complexes of *O*-dimethylated *para-tert*-butylcalix[4]arene are significantly longer at 2.60 to 2.64 Å.[28-29] The short U–O distance in **3** is likely a consequence of the rigidity of the xanthene backbone; for comparison, Th–$O_{diarylether}$ distances of 2.52-2.53 Å were observed in related [(XA_2)Th$(CH_2R)_2$] (R = $SiMe_3$ and Ph) complexes.[3,4] These Th–O distances are comparable with the U–O distance in **3**, after taking into consideration the greater ionic radius of Th^{IV} relative to U^{IV} (0.94 versus 0.89 Å).[30]

X-Ray quality crystals of [Li$(DME)_3$][$(TXA_2)UCl_3$]·DME (**4**·DME) were grown from DME/hexane at –30 °C (Figure 4, Table 1; two independent but isostructural molecules are present in the unit cell), and like the XA_2 analogue, complex **4** is a six coordinate trichloro 'ate' complex. However, in this case, the [Li$(DME)_3]^+$ counter-cation is not associated with the [$(TXA_2)UCl_3]^-$ anion in the solid state. As in complex **3**, the anionic N and Cl donors in **4** adopt an approximate trigonal bipyramidal arrangement, and

the neutral donor is coordinated between the two amido groups in the equatorial plane of the trigonal bipyramid.

Table 1. Crystallographic data collection and refinement parameters, and crystallographic data for complexes **3**-**6**.[a]

Structure	**3**	**4**·DME	**5**·4.5toluene	**6**
Empirical formula	$C_{59}H_{92}N_2O_7Cl_3KU$	$C_{126}H_{204}N_4O_{16}S_2Cl_6Li_2U_2$	$C_{82.50}H_{108}N_2O_3ClU$	$C_{59}H_{92}N_2O_6SCl_2LiU$
Formula weight	1324.83	2797.69	1449.19	1273.28
Temperature (K)	173(2)	173(2)	100(2)	120(2)
Crystal system	Orthorhombic	Triclinic	Monoclinic	Orthorhombic
Space group	P2(1)2(1)2(1)	P-1	P2(1)/c	Pbca
a (Å)	11.4562(16)	17.268(3)	14.402(2)	24.5716(11)
b (Å)	22.380(3)	17.302(3)	15.964(2)	20.4781(10)
c (Å)	25.144(3)	24.551(4)	29.638(5)	24.9710(12)
α (deg)	90	102.232(5)	90	90
β (deg)	90	91.523(4)	94.854(3)	90
γ (deg)	90	101.233(4)	90	90
Volume (Å^3)	6446.7(15)	7014(2)	6789.8(17)	12564.9(10)
Z	4	2	4	8
Crystal size (mm^3)	0.50 x 0.08 x 0.04	0.18 x 0.01 x 0.01	0.35 x 0.18 x 0.10	0.22 x 0.20 x 0.10
No. of reflections collected	151566	72839	63593	142930
No. of indep. reflections	19639	24567	11944	11334
θ range (deg)	1.82 to 30.54	1.54 to 25.00	1.38 to 25.00	2.08 to 25.22
Completeness to θ_{max} (%)	99.50	99.4	99.9	99.8
GOF on F^2	1.012	0.998	1.059	1.07
Final R_1 [I>2σ(I)] (%)	4.53	6.06	7.81	4.41
U(1)–N(1) [Å]	2.297(4)	2.355(6), 2.373(6)	2.340(8)	2.520(5)
U(1)–N(2) [Å]	2.306(4)	2.382(6), 2.363(6)	2.364(8)	2.504(5)
U(1)–E (E = S or O_{xant}) [Å]	2.465(3)	2.763(2), 2.779(2)	2.523(6) (O1)	2.825(1)
U(1)–Cl(1) [Å]	2.619(1) (in plane)	2.632(2), 2.619(3) (in plane)	2.689(3)	2.828(2) (μ-Cl)
U(1)–Cl(2) [Å]	2.597(1)	2.620(2), 2.625(2)	n.a.	2.714(1)
U(1)–Cl(3) [Å]	2.672(1) (μ-Cl)	2.629(2), 2.628(2)	n.a.	n.a.
U(1)–O_{DME} [Å]	n.a.	n.a.	2.580(6) (O2), 2.655(7) (O3)	2.782(4) (O1), 2.616(4) (O2)
K–Cl or Li–Cl [Å]	3.151(2)	n.a.	n.a.	2.42(1)
K–O or Li–O [Å]	2.55(1)-3.10(1)	n.a.	n.a.	1.98(1)-2.12(1)
C–E–C (E = S or O_{xant}) [°]	118.3(3)	96.8(3), 97.5(3)	117.2(7)	98.2(3)
U–E–C (E = S or O_{xant}) [°]	119.7(3), 119.8(3)	97.5(3), 97.6(2), 97.7(3), 98.5(3)	120.5(5), 121.0(5)	100.78(19), 101.32(18)

(a) For **4**·DME, the 2nd set of crystallographic data corresponds to the analogous bond lengths and angles in the 2nd independent molecule in the unit cell.

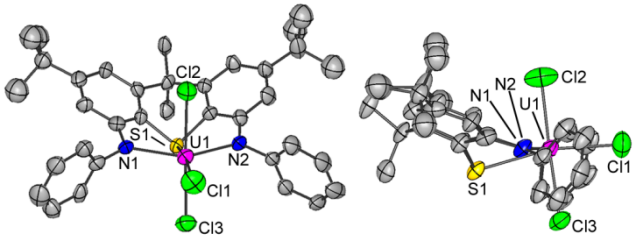

Figure 4. Molecular structure of **4**·DME with thermal ellipsoids at 50% probability. Hydrogen atoms, the $[Li(DME)_3]^+$ cation, isopropyl groups, and lattice solvent are omitted for clarity. Only one of the two independent molecules of **4** in the unit cell and only one orientation for the rotationally disordered *tert*-butyl groups is shown.

The U–Cl bonds in **4** [2.619(3)–2.632(2) Å] are longer than the $U–Cl_{terminal}$ bonds in **3** [2.597(1) and 2.619(1) Å] and shorter than $U–Cl_{bridging}$ in **3** [2.672(1) Å], suggesting that partial abstraction of one chloride in **3** leads to a compensatory shortening of the remaining U–Cl bonds. The U–N distances in **4** [2.355(6)-2.382(6) Å] are longer than those in **3** [2.297(4) and 2.306(4) Å], presumably due to improved donor ability of the thioether group in TXA_2 relative to the ether group in XA_2, the absence of an alkali metal–chloride interaction in **4**, and/or different structural constraints imposed by the rigid TXA_2 ligand framework.

As expected, the U–S distances in **4** [2.763(2), 2.779(2) Å] are longer than the U–O distance in **3** [2.461(2) Å].[31] However, the 0.31 Å difference in $U–S_{avg}$ and U–O bond lengths is less than the difference in the covalent radii of sulphur and oxygen (0.39 Å),[32] and the U–S distances in **4** are significantly shorter than those in all other structurally characterized uranium complexes of neutral sulphur-donor ligands (Figure 2). For example, U–S distances are 3.089(1) Å in $[Cp^*U^{IV}\{\kappa^6\text{-}B_3(Cat)_6\}(SMe_2)]$,[12] 3.09(1) and 3.04(1) Å in $[(\kappa^2\text{-}MeSCH_2CH_2SMe)U^{IV}(BH_3Me)_4]$,[13] 3.120(4)–3.275(4) Å in $[\{(MeBH_3)_4U^{IV}(\mu\text{-}THT)\}_2]$,[14] 2.986(5) Å in $[(C_5H_4Me)_3U^{III}(THT)]$,[15] 3.015(1)–3.078(1) Å in $[(\kappa^3\text{-}9S3)U^{III}I_3(NCMe)_2]$,[16] 3.013(3)–3.101(3) in $[(\kappa^6\text{-}18S6)U^{III}(BH_4)_2][BPh_4]$,[18] and 2.912(3)–2.937(3) in $[\{\kappa^3\text{-}HPhB(mim)_2\}_2U^{III}(THF)_3][BPh_4]$.[19] Ligand rigidity is likely to be a significant factor contributing to the remarkably short U–S distance in **4**. However, DFT calculations also highlight significantly greater covalency in U–S bonding versus U–O bonding (*vide infra*).

In contrast to the planar ligand backbone in **3** (C–O–C and C–O–U angles of 118–120°), the backbone of **4** is strongly bent with C–S–C and C–S–U angles of 97–98°, and a 41° angle between the planes of the thioxanthene aryl rings. Similar C–S–C angles (96–104°) have been observed in [Cp*U^{IV}{κ^6-$B_3(cat)_6$}(SMe_2)],[12] [(κ^2-$MeSCH_2CH_2SMe$)$U^{IV}(BH_3Me)_4$],[13] [$(C_5H_4Me)_3U^{III}$(THT)],[15] [(κ^3-9S3)$U^{III}I_3(NCMe)_2$],[16] and [(κ^6-18S6)$U^{III}(BH_4)_2$][BPh_4].[18] However, the C–S–U angles in **3** are uncommonly acute, with the sum of the C–S–U angles equal to 195–196°, compared with 213–232° in the literature complexes above. Acute C–S–U angles in **3** are likely favored to maximize the overall effectiveness of U–N and U–S bonding within the constraints imposed by the rigid TXA_2 ligand architecture [in particular, the larger atomic radius of sulfur relative to oxygen leads to much longer E···C(4) and E···C(5) distances in compound **3** than in compound **4** (2.33 versus 2.67 Å), so a bent ligand backbone is likely required to ensure comparable C(4)···C(5) and N(1)···N(2) distances in both compounds {the C(4)–C(5) distances in **3** and **4** are 4.65 and 4.74 Å, respectively, and the N(1)···N(2) distances in **3** and **4** are 4.16 and 4.33 Å, respectively}]. However, despite significant differences in the conformations of the XA_2 and TXA_2 ligands in **3** and **4**, both ligands adopt an approximately meridional rather than facial coordination mode.

^{1}H NMR spectra for **3** and **4** in d_8-THF show paramagnetically shifted peaks; between +20 and –10 for **3**, and between +55 and –20 ppm for **4**. The ^{1}H NMR spectrum of **3** is indicative of C_{2v} symmetry; for example, a single C*H*Me_2 signal was observed at 16.08 ppm, coupled to two CH*Me*$_2$ signals.[33] By contrast, and consistent with the bent thioxanthene backbone of the TXA_2 ligand, the ^{1}H NMR spectrum of **4** indicates C_s symmetry; two C*H*Me_2 signals were observed at 55.26, and 9.77 ppm, associated with four CH*Me*$_2$ signals. Addition of Tl[$B(C_6F_5)_4$] to a solution of **3** in d_8-THF resulted in immediate precipitation of a white solid (presumably TlCl) with no significant change in the ^{1}H NMR spectrum, indicating that the C_{2v} symmetry of **3** in THF is due to [$K(THF)_x$]Cl dissociation to form [(XA_2)UCl_2(THF)] with both chloro ligands in axial positions (cf. [(XA_2)$ThCl_2$(DME)]). By contrast, addition of Tl[$B(C_6F_5)_4$] to a solution of **4** in d_8-THF caused rapid decomposition.

Reduction to Uranium(III)

The CV of **3** in THF/$[NBu_4][B(C_6F_5)_4]$[34,35] showed an irreversible reduction peak at E_{pc} = –2.46 V vs $FeCp_2^{0/+1}$ (ν = 200 mVs^{-1}) which gave rise to a product wave with $E_{1/2}$ = –1.83 V. The TXA_2 analogue, **4**, displayed similar redox behavior; an irreversible reduction to uranium(III) at E_{pc} = –2.56 V associated with an irreversible product peak at E_{pa} = –1.83 V. The irreversibility of the primary redox processes is likely due to rapid chloride loss from the uranium(III) redox product, although rapid reaction of the uranium(III) redox product with the $[NBu_4][B(C_6F_5)_4]$ base electrolyte (present in 100 fold excess) cannot be ruled out.[36] In keeping with the ^{1}H NMR spectrum of **3** after treatment with $Tl[B(C_6F_5)_4]$ (*vide supra*), the CV of **3** was essentially unchanged after addition of 1 equiv. of $Tl[B(C_6F_5)_4]$ to precipitate TlCl.[37] The redox chemistry of **3** in THF is therefore attributed to $[(XA_2)UCl_2(THF)_x]$ rather than the $[(XA_2)UCl_3]^-$ anion, and dissociation of LiCl from **4** (to form $[(TXA_2)UCl_2(THF)_x]$) is also likely in THF. $[(L)UCl_2(THF)_x]$ (L = XA_2 and TXA_2) complexes therefore appear to be reduced at more negative potentials than $[Cp^*_2UCl_2]$ ($E_{1/2}$ = –1.85 V vs $FeCp_2^{0/+1}$) or $[(PNP^1)_2UCl_2]$ ($E_{1/2}$ = –2.19 V vs $FeCp_2^{0/+1}$).[9,38]

Reaction of **3** with 1.1 equiv. of potassium naphthalenide in DME, followed by centrifugation and crystallization from toluene/hexane at –30 °C provided $[(XA_2)U^{III}Cl(DME)]$·4.5toluene (**5**·4.5toluene) as dark green X-ray quality crystals. Similarly, reaction of **4** with potassium naphthalenide in DME and crystallization from DME/hexane at –30 °C resulted in a mixture of dark green X-ray quality crystals of $[(TXA_2)U(DME)Cl(\mu\text{-}Cl)Li(DME)_2]$ (**6**) and a red powder identified as **4** by ^{1}H NMR spectroscopy. Both **5** and **6** are extremely air sensitive, and complex **6** is also thermally unstable, decomposing slowly even at

–30 °C, which prevented isolation and NMR characterization of a pure bulk sample; UV-Visible-NIR spectra and elemental analyses were obtained on hand-picked samples of crystals.

Scheme 3. Synthesis of complexes **5** and **6**. *tert*-Butyl groups are omitted for clarity.

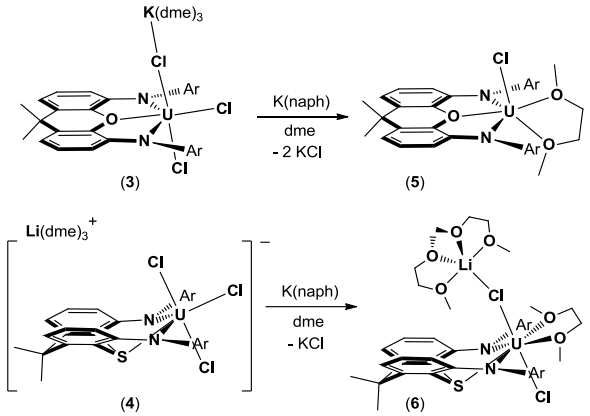

Complex **5** (Figure 5), unlike uranium(IV) XA_2 precursor **3**, is free from occluded alkali metal salt. A molecule of DME is also κ^2-coordinated to uranium with U–O bond lengths of 2.580(6) and 2.655(7) Å, and as is typical in 5*f*-element complexes of the XA_2 ligand,[3-5,39] the ligand backbone in complex **5** is planar. All uranium–XA_2 ligand bond lengths in **5** are 0.04–0.06 Å longer than those in complex **3**, consistent with the increased ionic radius of uranium(III) relative to uranium(IV) [for a coordination number of six: U^{4+} = 0.89 Å and U^{3+} = 1.03 Å].[30] At 2.689(3) Å, the U–Cl bond in **5** is also significantly longer than the U–$Cl_{terminal}$ bonds in **3** [2.597(1), 2.619(1) Å]. Uranium–ligand bond elongation has previously been observed for the uranium(III) compound in other uranium(III)/(IV) pairs, including $[Cp^*_2U(CN)_3]^{n-}$ (n = 1 and 2),[40] $[(\kappa^2\text{-dmpe})U(BH_4)_4]$ and $[(\kappa^2\text{-dmpe})_2U(BH_4)_3]$,[41] and $[U(\kappa^2\text{-SBT})_4]$ and $[U(\kappa^2\text{-SBT})_4(py)]^-$ (SBT = 2-mercaptobenzothiazolate).[42] However, bond elongation in the BH_4 and SBT examples may be due to an increase in coordination number in the uranium(III) complex, and a significant dependence of uranium-ligand bond lengths on metal oxidation state is not always observed. For example,

U–PR_3 and U–NAr_2 bonds in tri- and tetravalent uranium complexes of the PNP[1] monoanion were largely unaffected by changes in oxidation state.[9] All peaks in the ^{1}H NMR spectrum of **5** are localized between +10 to –10 ppm, and confirm that the approximate C_s symmetry of the solid state structure is maintained in solution. For example two C*H*Me_2 signals were observed at 1.68 and –2.17 ppm, coupled to four CH*Me*$_2$ signals at 0.26, –0.92, –2.04 and –8.69 ppm.

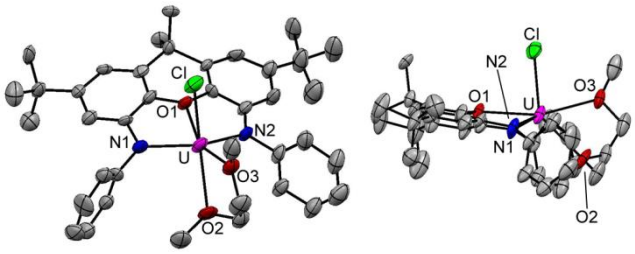

Figure 5. Molecular structure of complex **5**·4.5toluene with thermal ellipsoids at 50% probability. Hydrogen atoms, isopropyl groups, and lattice solvent are omitted for clarity.

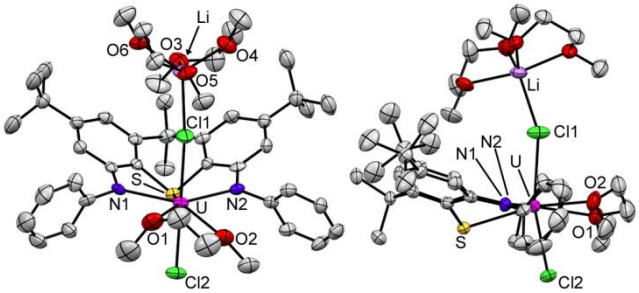

Figure 6. Molecular structure of complex **6** with thermal ellipsoids at 50% probability. Hydrogen atoms and isopropyl groups are omitted for clarity.

Heptacoordinate **6** (Figure 6) adopts a distorted pentagonal bipyramidal geometry at uranium, with angles of 62–86 ° between adjacent ligands in the pentagonal plane (the sum of the angles is 365°). One chloride ligand and one $ClLi(DME)_2$ fragment occupy the apical sites, and as in complex **4**, sulphur is strongly pyramidalized (C–S–C and C–S–U = 98–101°) and the thioxanthene ligand backbone adopts a butterfly conformation.

The geometry at lithium is trigonal bipyramidal with the bridging chloride occupying an equatorial site. The Li–Cl(1) bond length of 2.420(9) Å in **6** is somewhat longer than the Li–Cl distances of 2.30–2.35 Å in $[Cp^*_3Y(\mu\text{-}Cl)Li(THF)_3]$,[43] $[(2,6\text{-}Ph_2H_3C_6)_2SmCl(\mu\text{-}Cl)Li(THF)_3]$,[44] and $[(Ln\{N(SiMe_3)_2\}_2\{(\mu\text{-}Cl)Li(THF)_3\}\{\mu\text{-}Cl\})_2]$ (Ln = Pr, Nd, Sm), all of which exhibit a lithium cation bound via a single M–Cl–Li bridge (crystallographically characterized *f*-element complexes incorporating a M–Cl–$Li(DME)_2$ linkage are not available for comparison).[45] Of the two U–Cl bond lengths, U–Cl(1) is 0.11 Å longer than U–Cl(2) [2.828(2) vs 2.714(2) Å] due to coordination with lithium; a similar situation was observed in the solid state structure of complex **3**, in which a single chloro ligand bridges between uranium and potassium. Other structurally characterized actinide(III) complexes containing a U–Cl–Li linkage are $[\{\kappa^3\text{-}O(CH_2CH_2NAr)_2\}UCl(\mu\text{-}Cl)_2Li(THF)_2]$ (Ar = 2,6-diisopropylphenyl),[24] $[Cp"_2U(\mu\text{-}Cl)_2Li(THF)_2]$ and $[Cp"_2U(\mu\text{-}Cl)_2Li(\kappa^3\text{-}L)]$ (L = pentamethyldiethylenetriamine; Cp" = 1,3-bistrimethylsilylcyclopentadienyl).[46]

All uranium-ligand bond lengths in **6** are significantly longer than those in **4**. For example, the average U–N, $U\text{–}Cl_{terminal}$ and U–S distances are 0.144, 0.088 and 0.054 Å longer, respectively, in compound **6**. Nevertheless, at 2.825(1) Å, the U–S bond in **6** remains shorter than those reported for other uranium thioether complexes (*vide supra*).[47] The increase in uranium-ligand bond lengths from **4** to **6** can be attributed to the larger ionic radius of U^{III} relative to U^{IV}, combined with a higher coordination number in **6**.

The molecule of DME in **6** is asymmetrically bound, with U–O distances of 2.616(4) and 2.782(4) Å, presumably due to a combination of steric crowding at the metal centre and weak U–O_{DME} binding. Significant but much less pronounced asymmetry in DME binding was observed in complex **5**, and was also reported for the 7-coordinate thorium(IV) complex [$(XA_2)ThCl_2(DME)$] [Th–O_{DME} = 2.673(8) and 2.728(8) Å][3] and the uranium(III) calix[4]tetrapyrrole complex [(DME)U(μ-L)K(DME)] [L = $\{CH_2(C_4H_2N)\}_4$; C_4H_2N = 2,5-disubstituted pyrolide anion; U–O = 2.627(13) and 2.688(12) Å].[48]

UV-Visible and NIR spectra

UV-Visible and NIR spectra for uranium complexes **3**–**6** are shown in Figure 7. For complexes **3**-**6** as well as [$(XA_2)ThCl_2(DME)$], the most intense absorption lies above 30000 cm^{-1} (ε = 17000–30000 cm^{-1} M^{-1}), indicative of a ligand-centred (e.g. $n \rightarrow \pi^*$) transition. The absorption maxima for **4** and **6** (both 31950 cm^{-1}) are shifted bathochromically relative to those of **3** and **5** (33900 and 33350 cm^{-1}); the same trend in ν_{max} is observed for $H_2[TXA_2]$ (32100 cm^{-1}) and $H_2[XA_2]$ (33500 cm^{-1}).

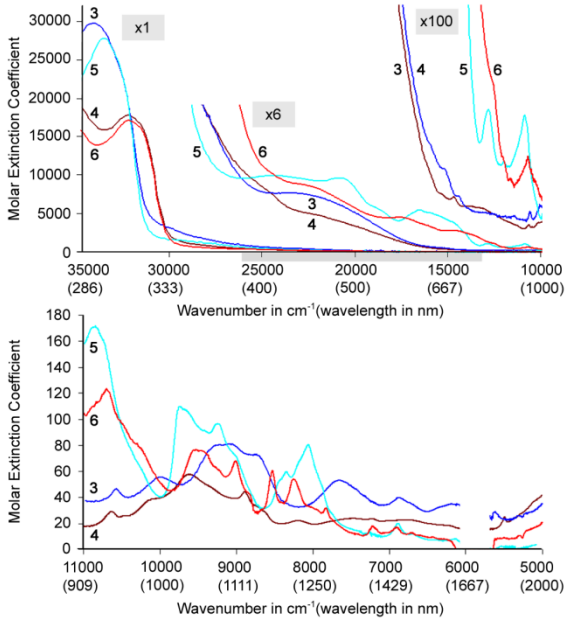

Figure 7. UV-Visible (top) and NIR (bottom) spectra for complexes **3** (dark blue line), **4** (dark red line), **5** (pale blue line) and **6** (red line) in toluene. UV-Visible spectra are shown at ×1, ×6 and ×100 magnification. The grey bar from ~ 26000 to 13000 cm^{-1} highlights the visible region (380 to 760 nm).

UV-visible spectra of **3-6** exhibit a broad shoulder between 25000 and 30000 cm^{-1}, and a broad medium intensity absorption between 25000 and 18000 cm^{-1}. Analogous features were not present for $[(XA_2)ThCl_2(DME)]$ (ν_{max} = 33800 cm^{-1}), $H_2[XA_2]$ or $H_2[TXA_2]$, consistent with *d–f* or MLCT transitions in **3-6**; the former seems more likely given the saturated nature of the donor groups attached to uranium. Additional broad absorptions ($\varepsilon \geq 500$ cm^{-1} M^{-1}) were observed for uranium(III) complexes **5** and **6** in the visible region; ν_{max} = 20900 and 16500 cm^{-1} for uranium(III) complex **5**, and ν_{max} = 17500 and 14600 cm^{-1} for complex **6**. Broad features in this energy range have been reported for $UI_3(THF)_4$ (ν_{max} = 20000 and 16700 cm^{-1}; ε = 1500-2000 cm^{-1} M^{-1}) and U^{III} in aqueous perchloric acid.[49]

The NIR region (13000 to 5000 cm^{-1}) for complexes **3**-**6** is dominated by low-intensity spin-forbidden *f*–*f* transitions resulting from the $5f^2$ and $5f^3$ electronic configurations of uranium(IV) and uranium(III), respectively. Invariably, the density of states from which these transitions derive is large, so specific assignments were not attempted. For complexes **3** and **4**, peaks in the NIR region are broad and poorly defined; similar spectra have been reported for a range of uranium(IV) complexes including $[U(NPh_2)_4]$,[25] various $[Cp^*_2U(N{=}CR^1R^2)_2]$ derivatives,[50] and $[U\{Fe(C_5H_4NSiMe_2{}^tBu)_2\}_2]$.[51] In the NIR spectra of uranium(III) complexes **5** and **6**, sharper but qualitatively similar features were also observed below 10000 cm^{-1}. However, complexes **5** and **6** exhibit additional *f*–*f* transitions between 13000 and 10000 cm^{-1} (ε 120–170 cm^{-1} M^{-1}; ν_{max} = 12750 and 10800 cm^{-1} for **5**; ν_{max} = ~12500 (shoulder) and 10700 cm^{-1} for **6**). Comparable absorptions were not observed for uranium(IV) complexes **3**, **4**, $[(PNP^1)_2UCl_2]$, $[(PNP^1)UCl_3(OPMe_3)_2]$, $[Cp^*_2UCl_2]$ or $[CpU(CH_2Ph)_3]$.[9] However, similar features have been reported for tervalent $[(PNP^1)_2UI]$, $[((PNP^1)UI_2(NC_5H_4{}^tBu\text{-}p)_2]$, $[Cp^*_2UI(THF)]$,[9] $[U\{N(SiMe_3)_2\}_3(NHC)]$ (NHC = tetramethylimidazol-2-ylidene),[52] $[U(NCMe)_9]I_3$,[53] $[NH_4][UBr_4]$ (solid),[54] $[UI_3(THF)_4]$, and $[UI_3(DME)_2]$.[55]

DFT Calculations

To gain insight into the nature of U–S and U–$O_{xanthene}$ bonding in complexes **3**-**6**, spin-unrestricted gas-phase DFT calculations (ADF, all-electron, TZP, ZORA, VWN, PW91) were carried out (calculations on **4** involved only the uranium anion since the $Li(DME)_3^+$ cation is not associated with the anion in the solid state). The geometries of all complexes were fully optimized without symmetry constraints using the ADIIS scheme[56] of Hu and Yang if necessary to achieve SCF convergence. In addition, analogous geometry optimizations were carried out for the hypothetical structures $[(XA_2)UCl_3]^-$ (**3B**), $[(TXA_2)UCl_2(DME)]^-$ (**6B**) and $[(TXA_2)UCl(DME)]$ (**6C**); **3B** is the direct analogue of **4**, and **6C** is the direct analogue of **5**.

Calculated structures for **3**-**6** closely match the experimentally determined solid-state structures, and Table 2 reports key computed bond lengths and angles (see Table 1 for crystallographically determined values). Importantly, all calculated U–O_{xant}, U–S, U–N and U–Cl bond lengths are within 3 % of the experimental values (U–O_{DME}, K–O_{DME} and Li–O_{DME} bonds were on average overestimated), and all bond angles around uranium were well reproduced. The calculations also successfully reproduced: (1) the extent to which the xanthene backbone is planar while the thioxanthene backbone is bent, (2) the large C–S–C and C–S–U angles in TXA_2 complexes **4** and **6**, (3) elongation of U–$Cl_{bridging}$ distances relative to U–$Cl_{terminal}$ bonds, (4) longer U–Cl and U–N bonds in 7-coordinate **6** relative to those in 6-coordinate **3**, **4** and **5**, and (5) longer U–N distances in TXA_2 complex **4** than in XA_2 complex **3**. However, calculations did not show significant U–N or U–Cl bond lengthening in complex **5** relative to complex **3**, and the U–E (E = O_{xant} or S) bonds in **5** and **6** are slightly shorter than those in **3** and **4**, rather than slightly longer as observed crystallographically.

Table 2. Calculated metal–ligand bond distances (Å) and angles (deg), Mayer bond orders, Mulliken atom–atom overlap populations (α+β), Mulliken spin density at uranium, and Hirshfeld charges.[a]

Structure	3	3B	4	5	6	6B	6C
U–N distance	2.340, 2.347	2.363, 2.365	2.416, 2.425	2.338, 2.356	2.514, 2.519	2.530, 2.533	2.386, 2.392
U–E distance	2.516 (E = O_{xant})	2.522 (E = O_{xant})	2.797 (E = S)	2.489 (E = O_{xant})	2.754 (E = S)	2.754 (E = S)	2.754 (E = S)
U–Cl distance	2.564, 2.611 (in plane), 2.722 (μ-Cl)	2.600, 2.619 (in plane), 2.625	2.608, 2.614, 2.623 (in plane)	2.625	2.652, 2.885 (μ-Cl)	2.704, 2.724	2.634
U–O_{DME} distance	n.a.	n.a.	n.a.	2.667, 2.839 (in plane)	2.713, 2.865	2.734, 2.906	2.682, 3.035 (in plane)
M'–Cl distance	3.141 (M' = K)	n.a.	n.a.	n.a.	2.436 (M' = Li)	n.a.	n.a.
M'–O distance	2.844–3.005	n.a.	n.a.	n.a.	2.063–2.233	n.a.	n.a.
C–E–C angle	118.3	118.4	97.1	117.1	96.9	97.2	96.1
U–E–C angle	118.6, 119.4	118.7, 119.4	98.7, 98.9	120.9, 121.1	103.4, 104.6	104.3, 104.9	105.3, 105.4
Mayer U–E b.o.	0.238 (E = O_{xant})	0.241 (E = O_{xant})	0.626 (E = S)	0.290 (E = O_{xant})	0.649 (E = S)	0.665 (E = S)	0.730 (E = S)
Mayer U–N b.o.	0.635, 0.623	0.602, 0.593	0.572, 0.566	0.594, 0.578	0.448, 0.437	0.431, 0.426	0.591, 0.579
Mayer U–Cl b.o.	1.050, 0.986 (in plane), 0.702 (μ-Cl)	0.992, 0.986 (in plane), 0.962	1.020, 0.986 (in plane), 0.963,	0.951	0.922, 0.491 (μ-Cl)	0.769, 0.764	0.950
Mayer U–O_{DME} b.o.	n/a	n/a	n/a	0.223, 0.148 (*cis* to Cl)	0.175, 0.165	0.172, 0.137,	0.218, 0.124 (*cis* to Cl)
Mayer M'–Cl b.o.	0.086 (M' = K)	n/a	n/a	n/a	0.262 (M' = Li)	n/a	n/a
Mull. U–E o.p.	0.087 (E = O_{xant})	0.100 (E = O_{xant})	0.444 (E = S)	0.148 (E = O_{xant})	0.444 (E = S)	0.457 (E = S)	0.534 (E = S)
Mull. U–N o.p	0.151, 0.146	0.158, 0.156	0.167, 0.165	0.140, 0.134	0.127, 0.138	0.148, 0.140	0.188, 0.177
Mull. U–Cl o.p.	0.474, 0.481 (in plane), 0.312 (μ-Cl)	0.475, 0.491 (in plane), 0.417	0.494, 0.497 (in plane), 0.424	0.487	0.482, 0.271 (μ-Cl)	0.411, 0.363	0.474
Mull. U–O_{DME} o.p.	n/a	n/a	n/a	0.121, 0.096 (*cis* to Cl)	0.089, 0.135	0.097, 0.092	0.117, 0.105 (*cis* to Cl)
Mull. M'-Cl o.p.	0.064 (M' = K)	n/a	n/a	n/a	0.243 (M' = Li)	n/a	n/a
Mull. s.d. at U	2.249	2.242	2.252	3.116	3.075	3.039	3.119
Hirsh. at U	---	0.511	0.484	0.516	---	---	0.506
Hirsh. at E	---	–0.053 (E = O_{xant})	0.140 (E = S)	–0.057 (E = O_{xant})	---	---	0.130 (E = S)
Hirsh. at O_{DME}	---	n/a	n/a	–0.083, –0.079	---	---	–0.093, –0.080
Hirsh. at N	---	–0.196, –0.196	–0.196, –0.196	–0.208, –0.207	---	---	–0.207, –0.204
Hirsh. at Cl	---	–0.267, –0.232, –0.191	–0.256, –0.217, –0.206	–0.247	---	---	–0.230

(a) b.o. = bond order; o.p. = overlap population; Mull. = Mulliken (α+β); s.d. = spin density; Hirsh. = Hirshfeld charge; M' = Li or K; 'in plane' refers to the plane containing N, U and E atoms; E = S or O_{xant}.

To gain more in-depth insight into the structures of **3**-**6**, **3B**, **6B** and **6C**, Mayer bond orders,[57] Mulliken atom-atom overlap populations,[58] and Hirshfeld charges[59] were examined (Table 2). These data highlight partial chloride abstraction by the alkali metal cation in **3** and **6** with a more pronounced difference in U–$Cl_{bridging}$ versus U–$Cl_{terminal}$ Mayer bond orders in 7-coordinate **6** (0.491 versus 0.922 in **6** compared with 0.702 versus 0.986 and 1.050 in **3**), presumably as a result of a more covalent M'–Cl (M' =

Li or K) interaction in **6** (the M'–Cl Mayer bond order is 0.262 in **6** versus 0.086 in **3**) combined with increased steric crowding at uranium. Steric effects are also likely to be responsible for an overall reduction in the metal–ligand Mayer bond orders in 7-coordinate **6** and **6B**, relative to 6-coordinate **6C**. As a consequence, the discussion below focuses on the 6-coordinate alkali metal-free structures **3B**, **4**, **5** and **6C**.

Uranium–terminal ligand Mayer bond orders in **3B**, **4**, **5** and **6C** lie in the following ranges: 1.02-0.95 for U–Cl, 0.73-0.63 for U–S, 0.60-0.57 for U–N, 0.29-0.24 for U–O_{xant}, and 0.22-0.12 for U–O_{DME}. Mayer bond orders for the U–S bonds in TXA_2 complexes **4** and **6C** are much higher than those for the U–O_{xant} bonds in **3B** and **5**, and are even higher than the U–N bond orders in Table 2. Similarly, the Mulliken atom-atom overlap populations are 0.444 and 0.534 for the U–S bonds in **4** and **6C**, compared with 0.100 and 0.148 for the U–O_{xant} bonds in **3B** and **5**, respectively. These data are indicative of significantly greater covalency in U–thioether bonding relative to U–ether bonding, although they cannot be used to assess the relative strengths of U–S and U–O bonding.

The Hirshfeld charges (Table 2) on S and O_{xant} are between 0.130 and 0.140 for S in **4** and **6C**, and between –0.053 and –0.057 for O_{xant} in **3B** and **5**. These charges are only slightly more positive than those in the free ligand anions and proligands (geometry optimized using the same basis set and functional); +0.075, +0.047, –0.087 and –0.098 for $[TXA_2]^{2-}$, $H_2[TXA_2]$, $[XA_2]^{2-}$, and $H_2[XA_2]$, respectively. The Hirshfeld charge on uranium lies between 0.48 and 0.52 in **3B**, **4**, **5** and **6C**.

Molecular orbital (MO) energy level diagrams for **3B** and **4** are shown in Figure 8, accompanied by selected MO isosurfaces for α-spin orbitals. In both **3B** and **4**, the HOMO-1 (α-spin), HOMO (α-spin) and LUMO are localized on uranium with greater than 90 % 5*f*-character, and orbitals involved in U–N and U–Cl bonding can clearly be observed. MOs associated with U–S bonding may also be identified for TXA_2 complex **4** (HOMO-2, HOMO-6 and HOMO-21). However, MOs involving a significant U–O_{xant} bonding contribution were not readily located for **3B**. Similarly, MOs involved in U–S bonding could be identified

in **6C**, whereas MOs engaged in U–O bonding were not located in **5** (see supporting information). These observations are consistent with more covalent U–SAr_2 bonding, relative to U–OAr_2 bonding, reinforcing the conclusions from Mayer bond orders. However, more detailed analysis of U–SAr_2 and U–OAr_2 bonding was hindered by the strongly delocalized nature of the relevant molecular orbitals.

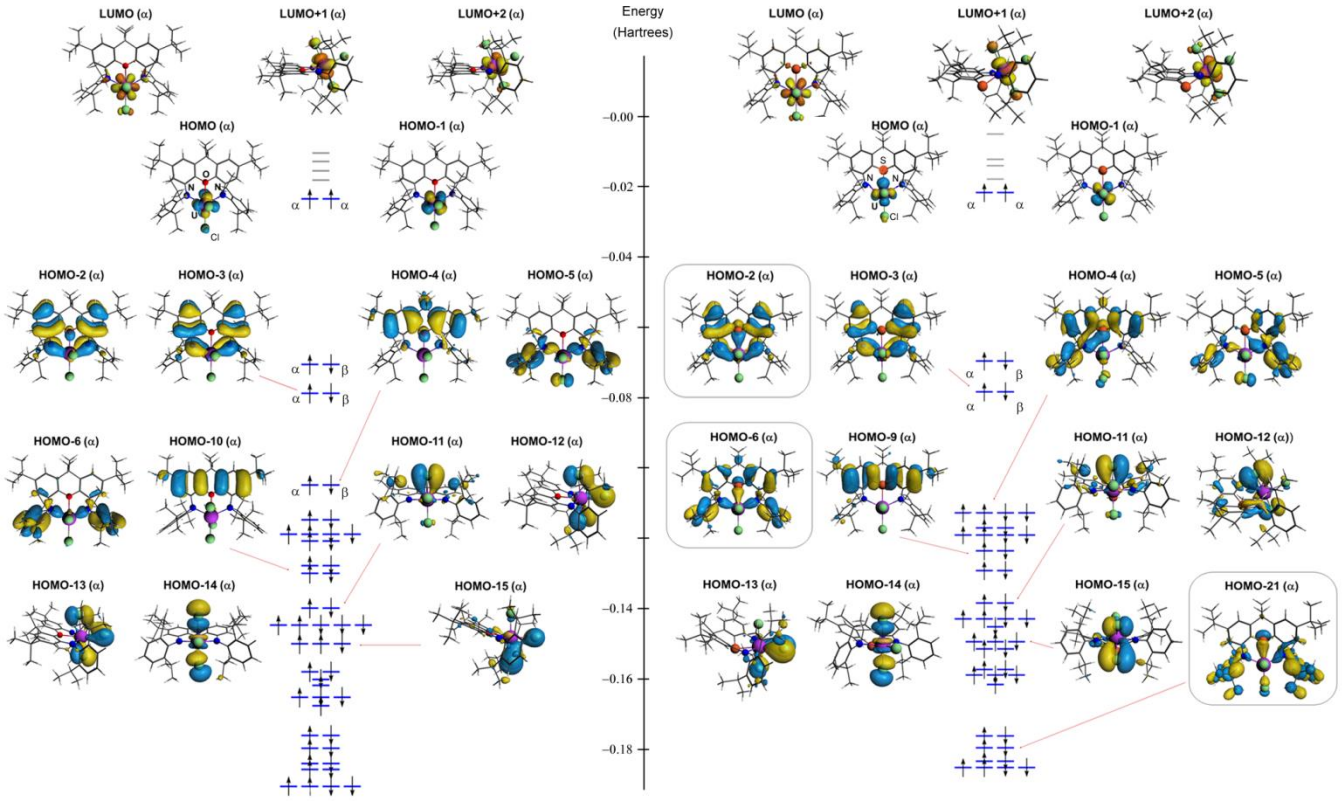

Figure 8. Molecular orbital energy level diagrams for $[(XA_2)UCl_3]^-$ (**3B**; left hand side) and $[(TXA_2)UCl_3]^-$ (**4**; right hand side) showing isosurfaces for selected α-spin MOs (isovalues set to 0.025 a.u.; for all doubly occupied orbitals in this figure, the α- and β-spin MO isosurfaces are qualitatively analogous; isosurfaces are shown for the LUMO+2 to the HOMO–6 and selected orbitals at lower energy, in particular those that appear to involve a significant U–O, U–S or U–N bonding contribution).

Atoms in Molecules (AIM) Calculations

Bader's Atoms In Molecules (AIM)[60,61] calculations have recently been used for the analysis of actinide–ligand bonding by Kaltsoyannis and Arnold,[62] Gagliardi and Liddle,[63] Michelini and Russo,[64] and Clark,[65] and in the current work, AIM analysis is of particular interest to probe in more detail the nature of U–SR_2 versus U–OR_2 bonding. AIM calculations were carried out on the results of Gaussian 09 single point calculations (all-electron, DZP-level ANO-RCC basis set for U and 6-31++G** basis set for all other atoms, DKH, VWN, PW91) using DZP geometry optimized structures from ADF (all uranium–ligand bond lengths are within 1.2 % of those in the TZP geometry optimized structures from ADF; tables of bond lengths and overlay diagrams are provided in the supplementary information).

Typical indicators of bond covalency are bond critical point electron densities (ρ_b) greater than 0.2 au, and significantly negative values for the Laplacian of the electron density at the bond critical point ($\nabla^2\rho_b$).[61] However, bonds involving atoms with diffuse valence electrons tend to have low ρ_b values [e.g. ~0.03 au for the unsupported M–M bonds in $Mn_2(CO)_{10}$ and $\{Co(CO)_3(AsPh_3)\}_2$].[66,67] Furthermore, characterization of bonds by the sign of $\nabla^2\rho_b$ becomes ambiguous for strongly polar or weak bonds; in such cases, $\nabla^2\rho_b$ will be small and of either sign.[61,67,68] These trends are exemplified in **3B**, **4**, **5** and **6C** (Table 3), where all uranium–ligand bonds exhibit small values of ρ_b (0.017 to 0.085 au) and small positive $\nabla^2\rho_b$ values (0.06 to 0.23 au).[69] Contour maps of $\nabla^2\rho$ are shown in Figure 9.

Table 3. Bond critical point topological properties of the electron density in **3B**, **4**, **5** and **6C**.[a]

Bonds in **3B**	ρ_b (au)	$\nabla^2\rho_b$ (au)	ε_b	$\delta_{(A-B)}$	G_b (au)	V_b (au)	H_b (au)
U–N	0.082,	0.219,	0.137,	0.638,	0.0703,	–0.0858,	–0.0155,
	0.081	0.219	0.168	0.633	0.0699	–0.0851	–0.0152
U–$Cl_{in\text{-}plane}$	0.068	0.163	0.007	0.765	0.0548	–0.0689	–0.0141
U–Cl_{axial}	0.069,	0.148,	0.021,	0.741,	0.0513,	–0.0655,	–0.0142,
	0.071	0.156	0.059	0.769	0.0545	–0.0700	–0.0155
U–O	0.043	0.181	0.036	0.267	0.0436	–0.0418	0.0017

Bonds in **4**	ρ_b (au)	$\nabla^2\rho_b$ (au)	ε_b	$\delta_{(A-B)}$	G_b (au)	V_b (au)	H_b (au)
U–N	0.071,	0.187,	0.400,	0.570,	0.0572,	–0.0676,	–0.0104,
	0.073	0.189	0.388	0.578	0.0585	–0.0698	–0.0113
U–$Cl_{in\text{-}plane}$	0.068	0.158	0.054	0.770	0.0536	–0.0676	–0.0141
U–Cl_{axial}	0.069,	0.151,	0.025,	0.779,	0.0523,	–0.0670,	–0.0146,
	0.071	0.152	0.016	0.778	0.0536	–0.0693	–0.0157
U–S	0.052	0.101	0.062	0.427	0.0338	–0.0422	–0.0084

Bonds in **5**	ρ_b (au)	$\nabla^2\rho_b$ (au)	ε_b	$\delta_{(A-B)}$	G_b (au)	V_b (au)	H_b (au)
U–N	0.083,	0.214,	0.232,	0.616,	0.0705,	–0.0875,	–0.0170,
	0.085	0.233	0.093	0.650	0.0758	–0.0934	–0.0176
U–Cl	0.068	0.160	0.110	0.714	0.0542	–0.0683	–0.0141
U–O_{xant}	0.048	0.198	0.340	0.285	0.0483	–0.0472	0.0011
U–$O_{DME\text{-}trans}$	0.035	0.128	0.220	0.241	0.0313	–0.0306	0.0007
U–$O_{DME\text{-}cis}$	0.023	0.090	0.628	0.177	0.0212	–0.0199	0.0013

Bonds in **6C**	ρ_b (au)	$\nabla^2\rho_b$ (au)	ε_b	$\delta_{(A-B)}$	G_b (au)	V_b (au)	H_b (au)
U–N	0.078,	0.206,	0.140,	0.739,	0.0656,	–0.0799,	–0.0142,
	0.078	0.210	0.100	0.739	0.0666	–0.0807	–0.0141
U–Cl	0.067	0.152	0.036	0.704	0.0522	–0.0664	–0.0142
U–S	0.056	0.121	0.160	0.463	0.0402	–0.0502	–0.0099
U–$O_{DME\text{-}trans}$	0.033	0.125	0.437	0.238	0.0304	–0.0296	0.0008
U–$O_{DME\text{-}cis}$	0.017	0.055	0.280	0.121	0.0134	–0.0131	0.0004

(a) The au for ρ is e/a_0^3 (1 au = 6.748 $e/Å^3$). The au for $\nabla^2\rho$ is e/a_0^5 (1 au = 24.098 $e/Å^5$). The au for G, V and H are e^2/a_0^4 (1 au = E_h/a_0^3 = 6.748 $E_h/Å^3$). a_0 = Bohr radius = 0.52918 Å. e = charge on an electron. E_h = hartree = e^2/a_0. (b) In **3** and **4B**, $Cl_{in\text{-}plane}$ is in the plane of the S and N atoms, while the Cl_{axial} ligands are *trans* to one another. In **5** and **6C**, O_{xant} = is the xanthene oxygen atom, $O_{DME\text{-}cis}$ is *cis* to Cl, and $O_{DME\text{-}trans}$ is more *trans* to Cl.

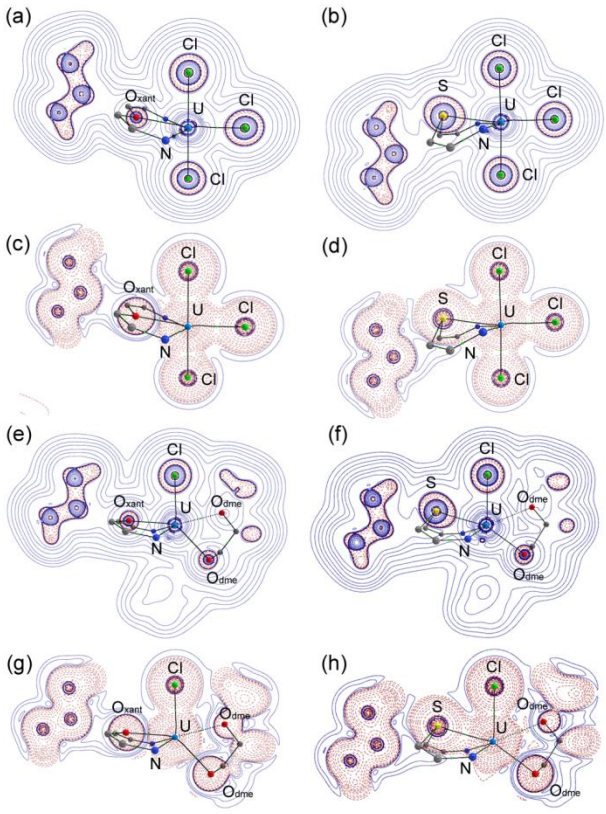

Figure 9. Contour maps of the Laplacian of the electron density ($\nabla^2\rho$) for **3B** (a), **4** (b), **5** (e) and **6C** (f) in the Cl–U–E plane (E = S or O_{xant}; the Cl–U–E plane in **3B** and **4** is defined using the Cl atom with the most acute Cl–U–E angle), and contour maps of the total energy density (*H*) for **3B** (c), **4** (d), **5** (g) and **6C** (h) in the Cl–U–E plane (E = S or O_{xant}). In all cases, solid blue lines represent zero and positive values, and dashed red lines represent negative values; contours are set to 0, ±0.001, ±0.002, ±0.004, ±0.008, ±0.02, ±0.04, ±0.08, ±0.2, ±0.4, ±0.8, ±2, ±4, ±8, ±20, ±40, ±80, ±200, ±400, and ±800 au. Bond paths with $\rho_b \geq 0.025$ au appear as solid lines, and bond paths $0.010 \geq \rho_b < 0.025$ au appear as dashed lines. Major contours to the left of the O_{xant} or S atom are due to carbon and hydrogen atoms within the CMe_2 group of the XA_2 or TXA_2 ligand backbone; these atoms also lie in the Cl–U–E plane.

The bond delocalization index (δ_{A-B}) provides an alternative means to measure the number of electron pairs shared by two atoms,[61] although the value of δ_{A-B} only matches the expected bond order if electron pairs are equally shared, and it does not reflect bond strength. For example, δ_{Na-Na} is 1.00 for Na_2, δ_{C-C} is 1.01, 1.90 and 2.85 in ethane, ethylene and acetylene, and δ_{C-O} is 1.58 and 1.80 in H_2CO and CO.[67] In **3B**, **4**, **5** and **6C** (Table 3) δ_{A-B} is 0.70-0.78 for U–Cl bonds, 0.57-0.74 for U–N bonds, 0.43 and 0.46 for U–S bonds, 0.27 and 0.29 for U–O_{xant} bonds, and 0.12-0.24 for U–O_{DME} bonds. The general trend in δ_{A-B} is consistent with decreasing bond covalency in the order U–Cl ≈ U–NR_2 > U–SR_2 > U–OR_2.

An additional bond critical point property that may be used to assess bond covalency is the total energy density (H_b) of Cremer and Kraka,[70] which is equal to the sum of the gradient kinetic energy density (G_b; always positive) and the potential energy density (V_b; always negative) [note that H_b is related to $\nabla^2\rho_b$ by the equation $(\hbar^2/4m)\nabla^2\rho_b = 2G_b + V_b = G_b + H_b$, where $\hbar$ is the reduced Planck constant and m is the mass of an electron]. In covalent bonds, as opposed to closed shell interactions, V_b dominates over G_b, and H_b will be negative.[61] In **3B**, **4**, **5** and **6C** (Table 3) negative H_b values are observed for all U–N, U–Cl and U–S bonds (–0.0084 to –0.0176), whereas positive H_b values are observed for all U–O bonds (0.0004 to 0.0017). The contour maps in Figure 9 clearly illustrate the absence of a region of positive H values near the midpoint of the U–S bond in **4** and **6C**, while in **3B** and **5** a region of positive H values (which includes the U–O bond critical points) is observed near the midpoint of the U–O bond. These data provide strong support for increased covalency in U–SR_2 bonds relative to U–OR_2 bonds, consistent with the observed bond delocalization indices and Mayer bond orders. These data do not however point to any clear trends in the extent of U–E (E = S or Oxant), U–N or U–Cl covalency in uranium(IV) complexes versus uranium(III) complexes.

Summary and Conclusions

A new extremely rigid, dianionic NSN-donor ligand, TXA_2, was prepared in protio- and lithiated form. Tetravalent and trivalent uranium complexes of TXA_2 and the NON-donor analogue, XA_2, were subsequently accessed, highlighting the suitability of both ligands for the synthesis of mono-ligated and κ^3-coordinated complexes. However, the thioether-ligated uranium(III) complex (**6**) demonstrated lower thermal stability than the XA_2 analogue (**5**). The xanthene ligand backbone in complexes of XA_2 is approximately planar, while the thioxanthene backbone in complexes of TXA_2 adopts a butterfly conformation. Both the XA_2 and TXA_2 ligands engage in approximately meridional coordination and appear to possess similar donor properties based on peak potentials for irreversible reduction of **3** and **4**.

ADF and AIM calculations point to significantly greater covalency in U–SAr_2 versus U–OAr_2 bonding. Increased covalency and/or the rigidity of the TXA_2 ligand are likely to be major factors responsible for the uncommonly short U–S distances and acute C–S–U angles in complexes **4** and **6**.

Experimental Section

General Details

General synthetic procedures have been reported elsewhere.[3-6,39] Deuterated solvents were purchased from ACP chemicals, UO_3 was purchased from Strem Chemicals, and $K[B(C_6F_5)_4]$ was purchased from Boulder Scientific. Thioxanthone, tetraglyme, $Pd(OAc)_2$, NaO*t*Bu, DPEPhos, KH (30 wt.% in mineral oil), K, naphthalene and $[NBu_4]Br$ were purchased from Sigma-Aldrich. 2,6-diisopropylaniline was purchased from Lancaster. Prior to use, solid KH was obtained by filtration and washing with hexanes, 2,6-diisopropylaniline was distilled from CaH_2, and tetraglyme was distilled from sodium/benzophenone. $H_2[XA_2]$, $[(XA_2)ThCl_2(DME)]$,[3] 4,5-dibromo-2,7-di-*tert*-butyl-9,9-dimethylthioxanthene,[20] and UCl_4[71]

were prepared by literature procedures. Before use, all traces of moisture and ethanol were eliminated from H_2XA_2 by stirring with NaH (4 equiv) in toluene for 16 hours at room temperature, followed by filtration and evaporation to dryness *in vacuo*. $[NBu_4][B(C_6F_5)_4]$ was prepared via a slight modification of the original literature procedure[72] (using $K[B(C_6F_5)_4]$ in place of $Li(OEt_2)_x[B(C_6F_5)_4]$) and dried thoroughly before use. Solutions of potassium naphthalenide were prepared immediately before use by stirring potassium (1.00*x* mmol) in DME (~10 mL per 0.15 mmol of K) with naphthalene (1.05*x* mmol) at room temperature until no solid remained (~30 min).

Combustion elemental analyses were performed on a Thermo EA1112 CHNS/O analyzer by Dr. Steve Kornic of this department. UV-Visible spectra were obtained on a Cary 50 UV/Visible Spectrometer and NIR spectra were obtained on a Thermo Scientific Nicolet 6700 FT-IR spectrometer using a quartz beam splitter and an InGaAs detector. NIR spectra were recorded for 1.0-3.0 mM solutions in toluene. UV-Visible spectra were recorded for 0.01-0.02, 0.2, and/or 1.0-3.0 mM solutions in toluene.

X-ray crystallographic analyses were performed on suitable crystals coated in Paratone oil and mounted on a SMART APEX II diffractometer with a 3 kW Sealed tube Mo generator in the McMaster Analytical X-Ray (MAX) Diffraction Facility. One of the two independent $[Li(DME)_3]^+$ countercations in the unit cell of **4**·DME, and 3.5 of the toluene molecules in **5**·4.5toluene (one is located on an inversion centre) were highly disordered, and could not be modeled satisfactorily, so were treated using the SQUEEZE routine.[73]

Electrochemical studies were carried out using a PAR (Princeton Applied Research) model 283 potentiostat (using PAR PowerCV software) in conjunction with a three-electrode cell under an argon atmosphere in an MBraun glove box. The auxiliary electrode was a platinum wire and the pseudo-reference electrode was a silver wire. The working electrode was a glassy carbon disk (3.0 mm diameter, Bioanalytical Systems) for compound **3** and a platinum disc (1.6 mm diameter, Bioanalytical Systems) for compound **4**. Solutions were 1 x 10^{-3} mol dm^{-3} in the test compound and 0.1 mol dm^{-3} in

$[N^nBu_4][B(C_6F_5)_4]$ as the supporting electrolyte. All CVs were referenced using $FeCp^*_2$ as an internal calibrant, all potentials are quoted versus $[FeCp_2]^{0/+1}$, and peak potentials for irreversible redox reactions are quoted at a scan rate of 200 mVs^{-1}. Under the conditions used, $E_{1/2}$ for $[FeCp^*_2]^{0/+1}$ is –0.48 V versus $[FeCp_2]^{0/+1}$.[74]

^1H, $^{13}C\{^1H\}$, DEPT-135, COSY, HSQC and HMBC NMR spectroscopy was performed on Bruker DRX-500 and AV-600 spectrometers. All ^1H NMR NMR spectra were referenced relative to $SiMe_4$ through a resonance of the employed deuterated solvent or protio impurity of the solvent; C_6D_6 (7.15 ppm) and d_8-THF (3.58, 1.73 ppm) for ^1H NMR, and C_6D_6 (128.0 ppm) for ^{13}C NMR. All NMR spectra were obtained at room temperature unless otherwise specified. Herein, *Ar* = 2,6-diisopropylphenyl, and the numbering scheme (CH^1, C^2, CH^3, C^4, C^{10} and C^{11}) for the thioxanthene/xanthene ligand backbones is shown in Figure 1.

H_2[TXA_2] (1)

A mixture of 4,5-dibromo-2,7-di-*tert*-butyl-9,9-dimethyl-thioxanthene (10.0 g, 20.14 mmol), 2,6-diisopropylaniline (7.60 mL, 40.28 mmol), NaO*t*Bu (5.42 g, 56.40 mmol), $Pd(OAc)_2$ (40 mg, 0.22 mmol) and DPEPhos (0.169 g, 0.30 mmol) in toluene (150 mL) was heated to 90 °C for 16 h. The reaction mixture was then quenched with water, extracted into toluene (3 x 50 mL), dried over $MgSO_4$, and concentrated to approximately 30 mL. Recrystallization from a hot ethanol/toluene (10:1) solution gave **1** as a pale cream solid which was dried *in vacuo* (8.22 g, 9.03 mmol, 70% yield). **^1H NMR (C_6D_6, 600 MHz):** δ 7.26 (t, 2H, Ar-CH_{para}, $^3J_{H,H}$ 7 Hz), 7.22 (d, 4H, Ar-CH_{meta}, $^3J_{H,H}$ 7 Hz), 7.17 (s, 2H, CH^1), 6.48 (s, 2H, CH^3), 5.87 (s, 2H, N*H*), 3.34 (sept, 4H, $^3J_{H,H}$ 7 Hz, C*H*Me_2), 1.78 (s, 6H, CMe_2), 1.22 (s, 18H, CMe_3), 1.19, 1.09 (d, $^3J_{H,H}$ 7 Hz, 2 x 12H, CHMe_2). **^{13}C NMR (C_6D_6, 150 MHz):** δ 150.58 (C^2), 147.68 (Ar-C_{ortho}), 145.07 (C^4), 144.62 (C^{10}), 135.96 (Ar-C_{ipso}), 127.95 (Ar-CH_{para}), 124.26 (Ar-CH_{meta}), 113.24 (C^{11}), 112.27 (CH^1), 107.86 (CH^3), 42.90 (CMe$_2$), 35.06 (CMe$_3$), 31.59 (CMe_3), 28.64 (CHMe$_2$), 25.76

(C*Me*$_2$), 24.67, 23.68 (CH*Me*$_2$). **Anal. Calcd. for $C_{47}H_{64}N_2S$:** C, 81.92; H, 9.36; N, 4.07 %. Found: C, 81.71; H, 8.94; N 4.42 %.

$Li_2(DME)_2[TXA_2]$ (2)

A 1.6 M solution of ^{n}BuLi in hexane (1.28 mL, 2.04 mmol) was added to **1** (700 mg, 1.02 mmol) in DME (30 mL) at –78 °C. The solution was allowed to warm to room temperature and was stirred for 12 hours. Solvent was then removed *in vacuo* to give **2** as a viscous yellow oil in quantitative yield. **^{1}H NMR (C_6D_6, 600 MHz):** δ 7.36 (d, 4H, Ar-C*H*$_{meta}$, $^3J_{H,H}$ 8 Hz), 7.21 (t, 2H, Ar-C*H*$_{para}$, $^3J_{H,H}$ 8 Hz), 6.86 (s, 2H, C*H*^{1}), 6.13 (s, 2H, C*H*^{3}), 3.61 (sept, 4H, $^3J_{H,H}$ 7 Hz, C*H*Me$_2$), 2.82 (s, 8H, OC*H*$_2$), 2.77 (s, 12H, O*Me*), 1.96 (s, 6H, C*Me*$_2$), 1.41 (s, 18H, C*Me*$_3$), 1.37, 1.19 (d, $^3J_{H,H}$ 7 Hz, 2 x 12H, CH*Me*$_2$). **^{13}C NMR (C_6D_6, 150 MHz):** δ 156.82 (*C*^{4}), 153.17 (Ar-*C*$_{ipso}$), 148.62 (*C*^{2}), 145.27 (Ar-*C*$_{ortho}$), 142.19 (*C*^{10}), 123.75 (Ar-*C*H$_{meta}$), 121.57 (Ar-*C*H$_{para}$), 109.7 (*C*^{11}), 108.19 (*C*H^3), 104.37 (*C*H^1), 69.98 (O*C*H$_2$), 57.41 (O*Me*), 41.18 (*C*Me$_2$), 35.03 (*C*Me$_3$), 32.10 (C*Me*$_3$), 29.17 (C*Me*$_2$), 27.71 (*C*HMe$_2$), 25.79, 24.93 (CH*Me*$_2$).

$[(XA_2)U^{IV}Cl_2(\mu\text{-}Cl)K(DME)_3]$ (3)

KH (0.130 g, 3.250 mmol) and $H_2(XA_2)$ (1.00 g, 1.486 mmol) in DME (60 mL) were stirred at room temperature overnight. To this mixture, solid UCl_4 (0.564 g, 1.484 mmol) was added, resulting in a colour change to reddish brown. After stirring for an additional 12 hours, the solution was evaporated to dryness *in vacuo* and the solid residue was redissolved in DME. The suspension was centrifuged to remove insoluble KCl and layered with *n*-hexanes at –30 °C. After 24 hours, X-ray quality red-orange crystals of **3**·DME were collected and dried *in vacuo* to provide 1.490 g of **3** (1.125 mmol, 75% yield). **^{1}H NMR (d_8-THF, 600.1 MHz):** δ 16.08 (broad s, 4H, C*H*Me$_2$), 9.69, –2.15 (s, 2 x 12H, CH*Me*$_2$), 3.43 (s, 18H, O*Me*), 3.27 (s, 12H OC*H*$_2$), 1.51 (s, 2H, Ar-*para*), –0.13 (s, 4H, Ar-*m*eta), –4.26 (s, 18H, C*Me*$_3$), –5.67, –19.99 (s,

2 x 2H, C*H*^{1} & C*H*^{3}), –6.08 (s, 6H, C*Me*$_2$). **UV-Vis-NIR** [ν in cm^{-1} (ε in L mol^{-1} cm^{-1})]: 33900 (30000), 23600 (1250), 10600 (45), 10050 (55), 9250 (80), 9120 (80), 8800 (70), 7700 (50), 6920 (40), 6230 (35), 5640 (25). **Anal. Calcd. for $C_{59}H_{92}N_2O_7Cl_3KU$:** C, 53.49; H, 7.00; N, 2.11 %. Found: C, 53.71; H, 6.83; N, 2.49 %.

[Li(DME)$_3$][(TXA$_2$)U^{IV}Cl$_3$] (4)

A solution containing 1.02 mmol of $Li_2(DME)_2[TXA_2]$ (**2**; prepared as described above) was added to UCl_4 (0.386 g, 1.02 mmol) in DME (approx. 15 mL) at –78 °C before warming to room temperature and stirring for 12 h to give a red solution. Solvent was removed *in vacuo* and DME (10 mL) was added, followed by centrifugation to remove lithium salts, and evaporation to dryness *in vacuo* to leave a tacky red solid. Hexane (~ 15 mL) was added, followed by sonication and evaporation to dryness *in vacuo*. Hexane (~ 10 mL) was again added, followed by centrifugation to collect **4** as a red powder (0.555 g, 0.42 mmol) in 42% yield. X-Ray quality crystals of **4**.DME were obtained from DME/hexane at –30 °C. **^{1}H NMR (*d*$_8$-THF, 200 MHz):** δ 55.26, 9.77 (broad sept., 2 x 2H, C*H*Me$_2$), 20.94, –3.63 (s, 2 x 2H, CH^{1} & CH^{3}), 17.54, 15.89 (d, $^{3}J_{H,H}$ 7 Hz, 2 x 2H, Ar-*meta*), 13.81 (app t, $^{3}J_{H,H}$ 7 Hz, 2H, Ar-*para*), 13.40, 8.29, 2.66, –4.43 (s, 4 x 6H, CHMe$_2$), 3.49 (s, 12H, OCH$_2$), 3.35 (s, 18H, OMe), 2.44 (s, 18H, CMe$_3$), –6.38, –14.44 (s, 2 x 3H, CMe$_2$). **UV-Vis-NIR** [ν in cm^{-1} (ε in L mol^{-1} cm^{-1})]: 31950 (19000), 25000 (broad shoulder), 2200 (broad shoulder), 10600 (25), 10100 (shoulder), 9600 (60), 8850 (40), 5540 (20). **Anal. Calcd. for $C_{59}H_{92}N_2SO_6Cl_3LiU$:** C, 54.14; H, 7.08; N, 2.14 %. Found: C, 53.72; H, 6.60; N, 2.07 %.

[(XA$_2$)U^{III}Cl(DME)]·toluene (5·toluene)

A solution of **3** (0.200 g, 0.151 mmol) in DME (10 mL) was added at –30 °C to a solution of potassium naphthalenide (0.154 mmol). The solution turned from green to dark brown within 15 min, and stirring

was continued for another 12 h, during which time the color changed to dark green. After evaporation to dryness *in vacuo*, the solid residue was redissolved in toluene, and the mixture was centrifuged to remove a small amount of insoluble material before layering with hexane at –30 °C. Dark green X-ray quality crystals of compound **5**·4.5toluene were obtained after two days at –30 °C and drying in vacuo provided **5**.toluene as a green-black powder (0.094 g, 0.091 mmol, 60% yield). **^{1}H NMR (C_6D_6, 600.1 MHz):** δ 9.93, 9.59 (s, 2 x 2H, CH^1 & CH^3), 8.48 (app t, 2H, $^3J_{H,H}$ 7 Hz, Ar-*para*), 8.15, 6.15 (d, 2 x 2H, $^3J_{H,H}$ 7 Hz, Ar-*meta*), 5.03, 2.08 (s, 2 x 3H, CMe_2), 3.33 (s, 4H, OCH_2), 3.01 (s, 6H, O*Me*), 2.89 (s, 18H, CMe_3), 1.64, –2.19 (broad s, 2 x H, C*H*Me_2), 0.25, –0.93, –2.12 and –8.70 (s, 4 x 6H, CHMe_2). **UV-Vis-NIR** [ν in cm^{-1} (ε in L mol^{-1} cm^{-1})]: 33350 (28000), 24400 (1700), 20900 (1700), 16500 (920), 12750 (180), 10800 (170), 9700 (110), 9200 (95), 8300 (60), 8050 (80), 6850 (20). **Anal. Calcd. for $C_{58}H_{80}N_2O_3ClU$:** C, 61.83; H, 7.16; N, 2.49 %. Found: C, 61.65; H, 7.22; N, 2.61 %.

[$(TXA_2)U^{III}Cl(DME)(\mu\text{-}Cl)Li(DME)_2$] (6)

A –30 °C solution of potassium naphthalenide (0.076 mmol) was added to a –30 °C solution of **3** (100 mg, 0.076 mmol) in DME (7 mL). The solution was allowed to warm to room temperature, and after 2 hours was evaporated to dryness *in vacuo*. The solid residue was redissolved in DME, and the mixture was centrifuged to remove a small amount of insoluble material before layering with hexane at –30 °C. After several days at –30 °C, dark green X-ray quality crystals of compound **6** (30 mg, 0.024 mmol, 32 % crude yield) were obtained together with a red powder identified as **4** by ^{1}H NMR spectroscopy. UV-Vis-NIR spectra and the elemental analysis were obtained using samples of manually selected crystals. **UV-Vis-NIR** [ν in cm^{-1} (ε in L mol^{-1} cm^{-1})]: 31950 (17000), 22500 (shoulder), 17500 (750), 14600 (500), 12500 (shoulder), 10700 (120), 9500 (75), 9000 (65), 8530 (60), 8240 (50), 7820 (30), 7200 (15) 6890 (15). **Anal. Calcd. for $C_{59}H_{92}N_2SO_6Cl_2LiU$:** C, 55.92; H, 7.32; N, 2.21 %. Found: C, 55.26; H, 7.35; N 1.98 %.

DFT and AIM Calculations

All structures were fully optimized with the ADF DFT package (SCM, version 2010.02)[75] using the default SCF convergence criterion (1×10^{-6}). The adiabatic local density approximation (ALDA) was used for the exchange-correlation kernel[76] and the differentiated static LDA expression was used with Vosko-Wilk-Nusair (VWN) parametrization.[77] All geometry optimizations were conducted using the zero-order regular approximation (ZORA)[78] for relativistic effects, and Perdew and Wang (PW91) exchange and correlation for the GGA part of the density functional.[79]

Preliminary geometry optimizations were conducted at the spin restricted level with frozen cores corresponding to the configuration of the preceding noble gas using a double-ζ basis set with one polarization function (DZP), and then using a triple-ζ basis set with one polarization function (TZP); the size and quality of ADF basis sets increases in the order SZ < DZ < DZP < TZP < TZ2P < QZ4P. These structures, respectively, were further refined at the DZP or TZP level using an all-electron basis set; initially using a spin restricted scheme, and then using a spin unsrestricted scheme. Note that ADF does not include a DZP basis set for uranium, so all DZP calculations use a TZP basis set for uranium and a DZP basis set for all other atoms.

For spin restricted calculations, we considered the highest spin state to be the ground state for all complexes (a triplet for U^{IV} and a quartet for U^{III}). All single point calculations were spin unrestricted. For spin unrestricted calculations, the Augmented Roothaan-Hall Direct Inversion Iterative Subspace (ADIIS) scheme of Hu and Yang was used if necessary to achieve SCF convergence.[56] Spin-orbit effects were not incorporated.

Visualization of computational results from ADF was performed using the ADF-GUI (SCM) or Discovery Studio Visualizer (Accelrys). Mayer bond orders[57] and Mulliken atom-atom overlap

populations were obtained using the ADF keyword EXTENDEDPOPAN or using the AOMix software package[80] (starting from unrestricted ADF single point calculation output files containing SFO MO coefficients and the SFO overlap matrix).

Atoms in molecules (AIM) analyses[60] were performed using the AIMAll program (professional version 10.12.13)[81] using formatted Gaussian 09 (G09)[82] checkpoint files as input (AIMAll requires the use of all-electron basis sets). For each atom, AIMAll calculations utilized: (a) the Proaim or 1st Order Promega integration methods, (b) high, very high or sky high outer angle basin quadratures, and (c) maximum integration radii between 15 and 18. These parameters ensured that the magnitude of the integration error for each atom was less than 1×10^{-3}, and typically below 1×10^{-4}. In AIMAll, Cremer and Kraka energy density (H) was accessed by plotting minus the Hamiltonian form of the electron kinetic energy density ($-K$), since $H = -K$.[81]

G09 checkpoint files were created by performing single point calculations[82] on geometry optimized structures that obtained from ADF as described above, but using an all-electron DZP basis set (in DZP geometry optimized structures, all uranium–ligand bond lengths at uranium are within 1.2 % of those in the TZP geometry optimized structures from ADF; these data are tabulated and overlay diagrams are provided in the supplementary information). G09 calculations employed PW91 exchange and correlation functionals,[79] the Vosko-Wilk-Nusair (VWN) Local Density Approximation,[77] a (26*s*23*p*17*d*14*f*5*g*3*h*)/[8*s*7*p*5*d*3*f*1*g*] (DZP level) all-electron ANO-RCC basis set for uranium,[83,84] and a 6-31++G** basis set for all other atoms. Scalar relativistic effects were included using the Douglas-Kroll-Hess (DKH) Hamiltonian.[83]

For **3B**, **5** and **6C**, but not **4**, we were also able to achieve SCF convergence using a (26*s*23*p*17*d*14*f*5*g*3*h*)/[9*s*8*p*6*d*4*f*2*g*1*h*] (TZP level) all-electron ANO-RCC basis set for uranium (using TZP geometry optimized structures from ADF).[84] Bond topological properties for **3B**, **5** and **6C** calculated

using the results of G09 calculations that employed a TZP ANO-RCC basis set are provided in the supplementary information (all trends mirror those obtained using a DZP ANO-RCC basis set).

Acknowledgement. D.J.H.E. thanks NSERC of Canada for a Discovery Grant and Canada Foundation for Innovation (CFI) and Ontario Innovation Trust (OIT) for New Opportunities Grants. N.R.A. and C.A.C. thank the Government of Ontario for an Ontario Graduate Scholarships (OGS) and NSERC of Canada for CGS-M (N.R.A.) and PGS-D (C.A.C.) Scholarships. We are grateful to Prof. Ignacio Vargas-Baca for help with ADF calculations and Prof. Gary Schrobilgen and Dr. Helene Mercier for help with Gaussian calculations. In addition, we are grateful to Prof. Paul Ayers for helpful discussions relating to various aspects of computational chemistry.

Electronic Supplementary Information (ESI) available: NMR spectra, UV-Vis spectra, CVs, calculated structures for **3**-**6**, **3B**, **6B**, **6C**, H_2[L] and L^{2-} (L = XA_2 and TXA_2), total electron density isosurfaces, full-page MO energy level diagrams for **3B**, **4**, **5** and **6C**, coordinates for TZP geometry optimized structures, and X-Ray crystallographic data for **3**-**6**. See DOI: 10.1039/b000000x/

References

1 (a) P. Maldivi, L. Petit, C. Adamo and V. Vetere, *Comptes Rendus Chimie*, 2007, **10**, 888; (b) K. L. Nash, C. Madic, J. N. Mathur and J. Lacquement, in Actinide Separation Science and Technology - The Chemistry of the Transactinide Elements, ed. L. R. Morss, N. M. Edelstein, J. Fuger, Springer: Dordrecht, The Netherlands, 3 edn.; 2006; vol. 4, pp. 2622.

2 (a) A. J. Gaunt, S. D. Reilly, A. E. Enriquez, B. L. Scott, J. A. Ibers, P. Sekar, K. I. M. Ingram, N. Kaltsoyannis and M. P. Neu, *Inorg. Chem.*, 2008, **47**, 29; (b) M. Roger, L. Belkhiri, T. Arliguie, P. Thuery, A. Boucekkine and M. Ephritikhine, *Organometallics*, 2008, **27**, 33.

3 C. A. Cruz, D. J. H. Emslie, L. E. Harrington, J. F. Britten and C. M. Robertson, *Organometallics*, 2007, **26**, 692.

4 C. A. Cruz, D. J. H. Emslie, L. E. Harrington and J. F. Britten, *Organometallics*, 2008, **27**, 15.

5 C. A. Cruz, D. J. H. Emslie, C. M. Robertson, L. E. Harrington, H. A. Jenkins and J. F. Britten, *Organometallics*, 2009, **28**, 1891.

6 C. A. Cruz, D. J. H. Emslie, H. A. Jenkins and J. F. Britten, *Dalton Trans.*, 2010, **39**, 6626.

7 (a) M. D. Fryzuk, J. B. Love, S. J. Rettig and V. G. Young, *Science*, 1997, **275**, 1445; (b) M. D. Fryzuk, *Can. J. Chem.*, 1992, **70**, 2839; (c) M. D. Fryzuk, T. S. Haddad and D. J. Berg, *Coord. Chem. Rev.*, 1990, **99**, 137; (d) M. D. Fryzuk and C. D. Montgomery, *Coord. Chem. Rev.*, 1989, **95**, 1.

8 L. C. Liang, *Coord. Chem. Rev.*, 2006, **250**, 1152.

9 T. Cantat, B. L. Scott, D. E. Morris and J. L. Kiplinger, *Inorg. Chem.*, 2009, **48**, 2114.

10 (a) S. J. Coles, P. G. Edwards, M. B. Hursthouse and P. W. Read, *Chem. Commun.*, 1994, 1967; (b) S. J. Coles, A. A. Danopoulos, P. G. Edwards, M. B. Hursthouse and P. W. Read, *Dalton Trans.*, 1995, 3401.

11 The chalcogen donor in TXA_2 is neutral, despite an overall charge of 2– on the ligand.

12 E. Barnea, T. Andrea, M. Kapon and M. S. Eisen, *J. Am. Chem. Soc.*, 2004, **126**, 5066.

13 R. Shinomoto, A. Zalkin, N. M. Edelstein and D. Zhang, *Inorg. Chem.*, 1987, **26**, 2868.

14 R. Shinomoto, A. Zalkin and N. M. Edelstein, *Inorg. Chim. Acta*, 1987, **139**, 91.

15 A. Zalkin and J. G. Brennan, *Acta Crystallogr. C*, 1985, **41**, 1295.

16 L. Karmazin, M. Mazzanti and J. Pecaut, *Chem. Commun.*, 2002, 654.

17 A. J. Gaunt, J. H. Matonic, B. L. Scott and M. P. Neu, *Recent Adv.Actinide Sci.*, 2006, **306**, 183.

18 T. Arliguie, L. Belkhiri, S. E. Bouaoud, P. Thuery, C. Villiers, A. Boucekkine and M. Ephritikhine, *Inorg. Chem.*, 2009, **48**, 221.

19 L. Maria, Â. Domingos and I. Santos, *Inorg. Chem.*, 2001, **40**, 6863.

20 D. J. H. Emslie, J. M. Blackwell, J. F. Britten and L. E. Harrington, *Organometallics*, 2006, **25**, 2412.

21 I. Korobkov, S. Gambarotta and G. P. A. Yap, *Angew. Chem. Int. Ed.*, 2003, **42**, 4958.

22 A. Zaeni, F. T. Edelmann, T. Kaehler and F. Olbrich, 2003, private communication to the Cambridge Structural Database, deposition number CCDC 178656.

23 H. Kawaguchi and T. Matsuo, *J. Organomet. Chem.*, 2005, **690**, 5333.

24 K. C. Jantunen, F. Haftbaradaran, M. J. Katz, R. J. Batchelor, G. Schatte and D. B. Leznoff, *Dalton Trans.*, 2005, 3083.

25 J. G. Reynolds, A. Zalkin, D. H. Templeton and N. M. Edelstein, *Inorg. Chem.*, 1977, **16**, 1090.

26 M. Silva, M. A. Antunes, M. Dias, Â. Domingos, I. C. dos Santos, J. Marcalo and N. Marques, *Dalton Trans.*, 2005, 3353.

27 R. E. Cramer, U. Engelhardt, K. T. Higa and J. W. Gilje, *Organometallics*, 1987, **6**, 41.

28 J. Old, A. A. Danopoulos and S. Winston, *New J. Chem.*, 2003, **27**, 672.

29 L. Salmon, P. Thuéry, Z. Asfari and M. Ephritikhine, *Dalton Trans.*, 2006, 3006.

30 R. D. Shannon, *Acta Cryst.*, 1976, **A32**, 751.

31 S. G. Murray and F. R. Hartley, *Chem. Rev.*, 1981, **81**, 365.

32 Covalent radii for sulphur and oxygen are 1.05(3) and 0.66(2) Å, respectively: B. Cordero, V. Gómez, A. E. Platero-Prats, M. Revés, J. Echeverría, E. Cremades, F. Barragán and S. Alvarez, *Dalton Trans.* 2008, 2832.

33 ^{1}H NMR spectra of complexes **3** and **4** in C_6D_6 were also consistent with C_{2v} and C_s symmetry, respectively.

34 For advantages of the $[NBu_4][B(C_6F_5)_4]$ anion as the base electrolyte in transition metal electrochemistry, see: (a) N. C. Ohrenberg, L. M. Paradee, R. J. DeWitte, D. S. Chong and W. E. Geiger, *Organometallics*, 2010, **29**, 3179; (b) J. C. Swarts, A. Nafady, J. H. Roudebush, S. Trupia and W. E. Geiger, *Inorg. Chem.*, 2009, **48**, 2156; (c) D. S. Chong, J. Slote and W. E. Geiger, *J. Electroanal. Chem.*, 2009, **630**, 28; (d) A. Nafady and W. E. Geiger, *Organometallics*, 2008, **27**, 5624; (e) D. Chong, D. R. Laws, A. Nafady, P. J. Costa, A. L. Rheingold, M. J. Calhorda and W. E. Geiger, *J. Am. Chem. Soc.*, 2008, **130**, 2692; (f) A. Nafady, T. T. Chin and W. E. Geiger, *Organometallics*, 2006, **25**, 1654; (g) F. Barriere, R. U. Kirss and W. E. Geiger, *Organometallics*, 2005, **24**, 48; (h) N. Camire, A. Nafady and W. E. Geiger, *J. Am. Chem. Soc.*, 2002, **124**, 7260; (i)

N. Camire, U. T. Mueller-Westerhoff and W. E. Geiger, *J. Organomet. Chem.*, 2001, **637**, 823; (j) ref 72; (k) ref 74.

35 For examples of the use of the $[NR_4][B(C_6F_5)_4]$ (R = ^{n}Bu or ^{i}Pr) base electrolytes in actinide electrochemistry, see: (a) R. K. Thomson, B. L. Scott, D. E. Morris and J. L. Kiplinger, *Comptes Rendus Chimie*, 2010, **13**, 790 and refs therein; (b) E. J. Schelter, R. L. Wu, B. L. Scott, J. D. Thompson, T. Cantat, K. D. John, E. R. Batista, D. E. Morris and J. L. Kiplinger, *Inorg. Chem.*, 2010, **49**, 924; (c) ref 9; (d) ref 38; (e) ref 50.

36 We were unable to obtain cyclic voltammograms for uranium(III) complexes **5** and **6**, perhaps due to rapid reaction with the 100-fold excess of $[NBu_4][B(C_6F_5)_4]$ base electrolyte.

37 The CV of complex **3** was also unchanged after addition of 10 equivalents of $[NBu_4]Cl$.

38 D. E. Morris, R. E. Da Re, K. C. Jantunen, I. Castro-Rodriguez and J. L. Kiplinger, *Organometallics*, 2004, **23**, 5142.

39 C. A. Cruz, T. Chu, D. J. H. Emslie, H. A. Jenkins, L. E. Harrington and J. F. Britten, *J. Organomet. Chem.*, 2010, **695**, 2798.

40 J. Maynadie, J. C. Berthet, P. Thuery and M. Ephritikhine, *Organometallics*, 2007, **26**, 4585.

41 J. Brennan, R. Shinomoto, A. Zalkin and N. Edelstein, *Inorg. Chem.*, 1984, **23**, 4143.

42 M. Roger, T. Arliguie, P. Thuery and M. Ephritikhine, *Inorg. Chem.*, 2008, **47**, 3863.

43 W. J. Evans, T. J. Boyle and J. W. Ziller, *Inorg. Chem.*, 1992, **31**, 1120.

44 D. J. Mihalcik, J. L. White, J. M. Tanski, L. N. Zakharov, G. P. A. Yap, C. D. Incarvito, A. L. Rheingold and D. Rabinovich, *Dalton Trans.*, 2004, 1626.

45 (a) B. Martin-Vaca, A. Dumitrescu, H. Gornitzka, D. Bourissou and G. Bertrand, *J. Organomet. Chem.*, 2003, **682**, 263; (b) H. X. Li, Q. F. Xu, J. X. Chen, M. L. Cheng, Y. Zhang, W. H. Zhang, J. P. Lang and Q. Shen, *J. Organomet. Chem.*, 2004, **689**, 3438; (c) H. X. Li, Z. G. Ren, Y. Zhang, W. H. Zhang, J. P. Lang and Q. Shen, *J. Am. Chem. Soc.*, 2005, **127**, 1122.

46 (a) P. C. Blake, E. Hey, M. F. Lappert, J. L. Atwood and H. M. Zhang, *J. Organomet. Chem.*, 1988, **353**, 307; (b) P. C. Blake, M. F. Lappert, J. L. Atwood and H. M. Zhang, *J. Chem. Soc. Chem. Commun.*, 1988, 1436.

47 In uranium(III) complex **5**, some U–S bonding contribution arising from diarylthioether π-acidity cannot be excluded: (a) H. B. Kraatz, H. Jacobsen, T. Ziegler, P. M. Boorman, *Organometallics*, 1993, **12**, 76; (b) G. E. D. Mullen, M. J. Went, S. Wocadlo, A. K. Powell and P. J. Blower, *Angew. Chem. Int. Ed.*, 1997, **36**, 1205.

48 I. Korobkov, S. Gambarotta and G. P. A. Yap, *Organometallics*, 2001, **20**, 2552.

49 D. Cohen and W. T. Carnall, *J. Phys. Chem.*, 1960, **64**, 1933.

50 E. J. Schelter, P. Yang, B. L. Scott, J. D. Thompson, R. L. Martin, P. J. Hay, D. E. Morris and J. L. Kiplinger, *Inorg. Chem.*, 2007, **46**, 7477.

51 M. J. Monreal, C. T. Carver and P. L. Diaconescu, *Inorg. Chem.*, 2007, **46**, 7226.

52 H. Nakai, X. L. Hu, L. N. Zakharov, A. L. Rheingold and K. Meyer, *Inorg. Chem.*, 2004, **43**, 855.

53 A. E. Enriquez, B. L. Scott and M. P. Neu, *Inorg. Chem.*, 2005, **44**, 7403.

54 E. Zych and J. Drożdżyński, *J. Less-Common Metals*, 1990, **161**, 233.

55 L. R. Avens, S. G. Bott, D. L. Clark, A. P. Sattelberger, J. G. Watkin and B. D. Zwick, *Inorg. Chem.*, 1994, **33**, 2248.

56 X. Hu and W. Yang, *J. Chem Phys* 2010, **132,** , 054109.

57 (a) A. J. Bridgeman, G. Cavigliasso, L. R. Ireland and J. Rothery, *J. Chem. Soc., Dalton Trans.*, 2001, 2095; (b) Mayer, I. *Chem. Phys. Lett.* **1983**, *97*, 270. Addendum **1985**, *117*, 396. (c) Mayer, I. *Int. J. Quantum Chem.* **1986**, *29*, 73. (d) Sannigrahi, A. B.; Kar, T. *Chem. Phys. Lett.* **1990**, *173*, 569.

58 (a) R. S. Mulliken, *J. Chem. Phys.*, 1955, **23**, 1833; (b) T. A. Albright, J. K. Burdett and M. H. Whangbo, in *Orbital Interactions in Chemistry*. John Wiley & Sons: 1985.

59 (a) F. L. Hirshfeld, *Theor. Chim. Acta*, 1977, **44**, 129; (b) E. R. Davidson and S. Chakravorty, *Theor. Chim. Acta*, 1992, **83**, 319; (c) C. F. Guerra, J. W. Handgraaf, E. J. Baerends and F. M. Bickelhaupt, *J. Comput. Chem.*, 2004, **25**, 189; (d) S. Saha, R. K. Roy and P. W. Ayers, *Int. J. Quantum Chem.*, 2009, **109**, 1790; (e) K. B. Wiberg and P. R. Rablen, *J. Comput. Chem.*, 1993, **14**, 1504.

60 R. F. Bader, in *Atoms in Molecules: A Quantum Theory*. Clarendon: New York, 1990.

61 C. F. Matta and R. J. Boyd, in *The quantum theory of atoms in molecules*. Wiley-VCH: Weinheim, 2007.

62 (a) P. L. Arnold, Z. R. Turner, N. Kaltsoyannis, P. Pelekanaki, R. M. Bellabarba and R. P. Tooze, *Chem. Eur. J.*, 2010, **16**, 9623; (b) M. J. Tassell and N. Kaltsoyannis, *Dalton Trans.*, 2010, **39**, 6719; (c) I. Kirker and N. Kaltsoyannis, *Dalton Trans.*, 2011, **40**, 124.

63 B. Vlaisavljevich, P. Miro, C. J. Cramer, L. Gagliardi, I. Infante and S. T. Liddle, *Chem. Eur. J.*, 2011, **17**, 8424.

64 E. Di Santo, M. D. Michelini and N. Russo, *Organometallics*, 2009, **28**, 3716.

65 A. E. Clark, J. L. Sonnenberg, P. J. Hay and R. L. Martin, *J. Chem. Phys.*, 2004, **121**, 2563.

66 L. J. Farrugia, P. R. Mallinson and B. Stewart, *Acta Crystallogr. B*, 2003, **59**, 234.

67 P. Macchi and A. Sironi, *Coord. Chem. Rev.*, 2003, **238**, 383.

68 (a) D. Stalke, *Chem. Eur. J.*, 2011, **17**, 9264; (b) F. Fuster and S. J. Grabowski, *J. Phys. Chem. A*, 2011, **115**, 10078.

69 Bond critical point elipticity values (ε_b; a measure of the extent to which electron density is preferentially accumulated in a given plane containing the bond path; 0.00 in ethane and acetylene, 0.23 in benzene and 0.45 in ethylene) are often not meaningful for very polar bonds, and as a result, the ε_b values in Table 3 do not follow any clear trend. See refs 61 and 68a.

70 (a) D. Cremer and E. Kraka, *Croat. Chem. Acta*, 1984, **57**, 1259; (b) D. Cremer and E. Kraka, *Angew. Chem. Int. Ed. Engl.*, 1984, **23**, 627.

71 J. L. Kiplinger, D. E. Morris, B. L. Scott and C. J. Burns, *Organometallics*, 2002, **21**, 5978.

72 R. J. LeSuer, C. Buttolph and W. E. Geiger, *Anal. Chem.*, 2004, **76**, 6395.

73 P. V. D. Sluis and A. L. Spek, *Acta Crystallogr.* , 1990, **A46**, 194.

74 F. Barriere and W. E. Geiger, *J. Am. Chem. Soc.*, 2006, **128**, 3980.

75 (a) ADF2010, SCM, Theoretical Chemistry, Vrije Universiteit, Amsterdam, The Netherlands, http://www.scm.com/. (b) G. te Velde, F. M. Bickelhaupt, S. J. A. van Gisbergen, C. Fonseca Guerra, E. J. Baerends, J. G. Snijders and T. Ziegler, *J. Comput. Chem.*, **2001**, *22*, 931. (c) C. Fonseca Guerra, J. G. Snijders, G. te Velde and E. J. Baerends, *Theor. Chem. Acc.*, **1998**, *99*, 391.

76 (a) S. J. A. van Gisbergen, J. G. Snijders and E. J. Baerends, *Phys. Rev. Lett.*, 1997, **78**, 3097; (b) S. J. A. van Gisbergen, J. G. Snijders and E. J. Baerends, *J. Chem. Phys.*, 1998, **109**, 10644.

77 S. H. Vosko, L. Wilk and M. Nusair, *Can. J. Phys.*, 1980, **58**, 1200.

78 (a) E. van Lenthe, E. J. Baerends and J. G. Snijders, *J. Chem. Phys.*, 1993, **99**, 4597; (b) E. van Lenthe, E. J. Baerends and J. G. Snijders, *J. Chem. Phys.*, 1994, **101**, 9783; (c) E. van Lenthe, A. Ehlers and E.-J. Baerends, *J. Chem. Phys.*, 1999, **110**, 8943; (d) E. van Lenthe, J. G. Snijders and E. J. Baerends, *J. Chem. Phys.*, 1996, **105**, 6505; (e) E. van Lenthe, R. van Leeuwen, E. J. Baerends and J. G. Snijders, *Int. J. Quantum Chem.*, 1996, **57**, 281.

79 (a) J. P. Perdew, *Phys. Rev. B*, 1986, **33**, 8822; (b) J. P. Perdew and Y. Wang, *Phys. Rev. B*, 1992, **45**, 13244.

80 (a) S. I. Gorelsky and A. B. P. Lever, *JOMC*, 2001, **635**, 187; (b) *AOMix: Program for Molecular Orbital Analysis*, http://www.sg-chem.net/, University of Ottawa, version 6.4, 2010.

81 T. A. Keith, AIMAll (Version 10.12.13), 2010 (http://aim.tkgristmill.com/).

82 *Gaussian 09 (Revision B.01)*. M. J. Frisch, G. W. Trucks, H. B. Schlegel, G. E. Scuseria, M. A. Robb, J. R. Cheeseman, G. Scalmani, V. Barone, B. Mennucci, G. A. Petersson, H. Nakatsuji, M. Caricato, X. Li, H. P. Hratchian, A. F. Izmaylov, J. Bloino, G. Zheng, J. L. Sonnenberg, M. Hada, M. Ehara, K. Toyota, R. Fukuda, J. Hasegawa, M. Ishida, T. Nakajima, Y. Honda, O. Kitao, H. Nakai, T. Vreven, J. A. Montgomery, Jr., J. E. Peralta, F. Ogliaro, M. Bearpark, J. J. Heyd, E. Brothers, K. N. Kudin, V. N. Staroverov, R. Kobayashi, J. Normand, K. Raghavachari, A. Rendell, J. C. Burant, S. S. Iyengar, J. Tomasi, M. Cossi, N. Rega, N. J. Millam, M. Klene, J. E. Knox, J. B. Cross, V. Bakken, C. Adamo, J. Jaramillo, R. Gomperts, R. E. Stratmann, O. Yazyev, A. J. Austin, R. Cammi, C. Pomelli, J. W. Ochterski, R. L. Martin, K. Morokuma, V. G. Zakrzewski, G. A. Voth, P. Salvador, J. J. Dannenberg, S. Dapprich, A. D. Daniels, Ö. Farkas, J. B. Foresman, J. V. Ortiz, J. Cioslowski, D. J. Fox, Gaussian, Inc., Wallingford CT, 2009.

83 The ANO-RCC basis set (Gaussian94 format) was obtained from the EMSL basis set library on the Basis Set Exchange database (version 1.2.2): https://bse.pnl.gov/bse/portal. (a) D. J. Feller, *Comp. Chem.* 1996, **17**, 1571. (b) K. L. Schuchardt, B. T. Didier, T. Elsethagen, L. Sun, V, Gurumoorthi, J. Chase, J. Li and T. L. Windus, *J. Chem. Inf. Model.* 2007, **47**, 1045.

84 B. O. Roos, R. Lindh, P.-A. Malmqvist, V. Veryazov and P.-O. Widmark, *Chem. Phys. Lett.*, 2005, **409**, 295.

Manuscript Title: Rigid NON- and NSN-Ligand Complexes of Tetravalent and Trivalent Uranium: Comparison of U–OAr_2 and U–SAr_2 Bonding

TOC Text (20-30 words)

Uranium(III) and (IV) complexes of extremely rigid, dianionic NON-donor and NSN-donor ligands have been prepared, and the extent of covalency in U–SAr_2 versus U–OAr_2 bonding was assessed using DFT and Atoms in Molecules calculations.

TOC GRAPHIC (max 8 x 4cm)